AD-A238 642

MENTATION PAGE

Form Approved
OMB No. 0704-0188

2. REPORT DATE	3. REPORT TYPE AND DATES COVERED
	FINAL 01 Sep 90 TO 30 Apr 91

4. TITLE AND SUBTITLE

An Optically Activated Modulator and GaAs-GaAlAs Compound Semiconductor Channel Waveguide

5. FUNDING NUMBERS

F49620-90-C-0068

6. AUTHOR(S)

Dr Chen

7. PERFORMING ORGANIZATION NAME(S) AND ADDRESS(ES)

Physical Optics Corporation
2545 West 237th Street, Suite B
Torrance, CA 90505

8. PERFORMING ORGANIZATION REPORT NUMBER

AFOSR-TR- 91 0664

9. SPONSORING / MONITORING AGENCY NAME(S) AND ADDRESS(ES)

AFOSR/NE
Bldg 410
Bolling AFB Washington DC 20332-6448
Dr. Alan E. Craig

10. SPONSORING / MONITORING AGENCY REPORT NUMBER

SDI 1602/F1

11. SUPPLEMENTARY NOTES

12a. DISTRIBUTION / AVAILABILITY STATEMENT

APPROVED FOR PUBLIC RELEASE: DISTRIBUTION IS UNLIMITED

12b. DISTRIBUTION CODE

13. ABSTRACT (Maximum 200 words)

We proposed and then developed for the first time an optically activated modulator (OAM) and modulator array on GaAs-GaAlAs compound semiconductor channel waveguides. A channel waveguide device with an optical activation window of 5 um in diameter was fabricated. Optical activation was produced by using HeNe 631.8 nm wavelength as the free-carrier generator and a 1.3 um laser as the signal carrier. Thirty-three percent modulation depth was observed and 10^{-2} index modulation was experimentally confirmed on an OAM working in the phase modulation regime. OAMs working in both phase- and cutoff-modulation regimes were theoretically determined by considering the fluctuation of the waveguide confinement factor. 8.2dB modulation depth was observed on an OAM working at the cutoff regime. Furthermore, the activation source is in the mW power region which significantly reduces the size and cost of all optical switching devices.

14. SUBJECT TERMS	15. NUMBER OF PAGES
	16. PRICE CODE

17. SECURITY CLASSIFICATION	18. SECURITY CLASSIFICATION	19. SECURITY CLASSIFICATION	20. LIMITATION OF ABSTRACT
UNCLASSIFIED	UNCLASSIFIED	UNCLASSIFIED	UNLIMITED

AN OPTICALLY ACTIVATED MODULATOR AND GaAs/GaAlAs COMPOUND SEMICONDUCTOR CHANNEL WAVEGUIDE

CONTRACT NO. F49620-90-C-0068

FINAL REPORT

April 30, 1991

Period of Performance: 9-1-90 to 4-30-91

Sponsor:

Strategic Defense Initiative

Contractor:

Physical Optics Corporation
2545 West 237th Street, Suite B
Torrance, California 90505
(213) 530-1416

Principal Investigator:

Ray Chen, Ph.D.

ABSTRACT

We proposed and then developed for the first time an optically activated modulator (OAM) and modulator array on GaAs-GaAlAs compound semiconductor channel waveguides. A channel waveguide device with an optical activation window of 5 μm in diameter was fabricated. Optical activation was produced by using a HeNe 632.8 nm wavelength as the free-carrier generator and a 1.3 μm laser as the signal carrier. Thirty-three percent modulation depth was observed and 10^{-2} index modulation was experimentally confirmed on an OAM working in the phase modulation regime. OAMs working in both phase- and cutoff-modulation regimes were theoretically determined by considering the fluctuation of the waveguide confinement factor. 8.2 dB modulation depth was observed on an OAM working at the cutoff regime. Furthermore, the activation source is in the mW power region which significantly reduces the size and cost of all optical switching devices.

Finally, both SDIO-mission related and civilian applications will be found for this concept. These applications include high speed laser wavelength and incident direction sensors, GaAs-OAM-based IR countermeasure systems, low threshold all-optical crossbar switching devices, optical gates (NOT, OR, AND), data sampling, generation of very short optical pulses and time division multiplexing (TDM) and demultiplexing.

TABLE OF CONTENTS

		Page
LIST OF FIGURES		iv
LIST OF TABLES		v
1.0	INTRODUCTION	1
2.0	PRINCIPLE OF OPERATION AND DEVICE STRUCTURE	2
2.1	The Working Principle	3
2.2	Device Structure for Comparison All-Optical and Linear E-O Effects	6
2.3	Device Fabrication	8
3.0	PERFORMANCE OF THE MODULATOR AND THE MODULATOR ARRAY	11
3.1	Experimental Setup	11
3.2	Optically Activated Phase Modulator	13
3.3	Waveguide Design Considerations	17
3.4	Optically Activated Cutoff Modulator	21
3.5	Modulation Speed	26
4.0	FURTHER APPLICATIONS	33
4.1	High-Speed Laser Wavelength and Incident Direction Sensors	33
4.2	GaAs-OAM-Based IR Countermeasure System	34
4.3	Low Threshold All-Optical Crossbar Switching Devices	35
4.4	Optical Gates	37
4.5	Data Sampling and Encoding, Generation of Very Short Optical Pulses, and Time Division Multiplexing	40
5.0	CONCLUSIONS	45
6.0	REFERENCES	46

LIST OF FIGURES AND TABLES

Figure 1 Basic Structure of Optically Activated Modulator on GaAs..... 3
Figure 2 Rotation of Principal Axes of GaAs Due to the Existence of an Electric Field..... 7
Figure 3 0.5 mm Electrode on a GaAs/GaAlAs Channel Waveguide and 5 μm Diameter Window for Optical Activation on a Single-Mode GaAs/GaAlAs Channel Waveguide..... 9
Figure 4 Illustration of One of the Cleaved End Faces of the Modulator Array..... 10
Figure 5 Fully Packaged Optically-Activated Modulator (OAM) on..... 10
Figure 6 Setup for OAM on GaAs/GaAlAs Channel Waveguide..... 12
Figure 7 Photograph of the Window for Optical Activation (5 μm in Diameter)..... 12
Figure 8 Near-Field Pattern of the Single-Mode Guided Wave from GaAs/GaAlAs Channel Waveguide. (a) Single-Channel and (b) Channel Waveguide Array..... 13
Figure 9 Transmission (I_t/I_i) of the GaAs OAM as a Function of Phase Shift with Waveguide Propagation Loss as a Parameter..... 15
Figure 10 Optically Activated Modulator: Top Trace = 0.633 μm Modulating Light Source, Bottom Trace = Modulated 1.3 μm Guided Wave (Modulation Speed 4 kHz)
Figure 11 Photo-Induced Phase Shift in the Guided Light Versus Modulating Light Power with Interaction Length of 5 μm..... 16
Figure 12 33% Modulation Depth of the 1.3 μm Guided Wave Throughput Generated Directly from a 0.5 mm Electrode with 10 Volt Peak to Peak Value at 4 kHz..... 16
Figure 13 Detection of the 1.3 μm Output Signal from the GaAs Channel Waveguide..... 17
Figure 14 Propagating Mode Profiles Along the Transverse Direction of the GaAs Waveguide (GaAs-$Ga_{0.93}Al_{0.07}As$). The Increase of the Evanescent Wave is Clearly Seen..... 19
Figure 15 Equal Electrical Field Topology of the Propagating Modes of the GaAs Waveguide (GaAs-$Ga_{0.93}Al_{0.07}As$) Corresponding to Figure 14..... 20
Figure 16 Confinement Factors as a Function of Effective Indices of the GaAs Waveguide (GaAs-$Ga_{0.93}Al_{0.07}As$)..... 21
Figure 17 Optically Activated Modulation (Bottom Trace) by Pulsing the Activation Light (Top Trace). Modulation Frequency 4 kHz..... 22
Figure 18 I-V Curve of the Schottky Diode
Figure 19 Amplification of Modulated Light as a Function of Reverse Bias Voltage with 632.8 nm Laser Shining on the Waveguide Surface..... 24
Figure 20 I-V Curve with 4 kHz Chopped Frequency..... 24
Figure 21 Induced Current as a Function of Reverse Bias Voltages With and Without a HeNe Laser (632.8 nm) Shining On the Window Area of the GaAs-GaAlAs Ridge Channel Waveguide..... 25
Figure 22 Modulated IR Guided Wave..... 26
Figure 23 (a) Device Package of the GaAs-GaAlAs Single-Mode Optically-Activated Modulator and (b) Equivalent Circuit of the Device Package..... 28
Figure 24 Compositional Dependence of the Direct Energy Gap and Indirect Energy Gap X and L for $Ga_{1-x}Al_xAs$..... 29
Figure 25 Device Capacitance as a Function of the Reverse Bias Voltage..... 30

Figure 26 Computer Simulated Results of the Voltage Transfer Function of the Equivalent Circuit Shown in Figure 23 (V_1 and V_{out} are Defined in Figure 23(b)).....31
Figure 27 Computer Simulated Results of the Phase Response as a Function of the Input rf Frequency.....32
Figure 28 High Speed Laser Wavelength and Incident Direction Sensor 34
Figure 29 GaAs-OAM Based IR Countermeasure System.....35
Figure 30 Low Threshold All Optical Crossbar Switching Device.....36
Figure 31 Optical OR Gate Using GaAs OAM Working in the Phase Modulation Regime.....37
Figure 32 Electrode Arrangement for Logic Gate Applications.....38
Figure 33 The Measured Results of Optical OR Gate.....39
Figure 34 Electrode Arrangement for Multiple-Channel Applications of the GaAs-GaAlAs Heterostructure Cutoff Modulator Array.....41
Figure 35 The Calculated Results of the Jitter-Free Optical Pulse.....42
Figure 36 Calculated Pulse Width as a Function of Fundamental Mode Microwave Frequency.....43
Figure 37 The Multiplexing of Multi-Electrical Pulse Trains 44
Figure 38 Demultiplexing of the TDM Signals Using the Proposed OAM.....45

Table 1 Demonstrated Features of the GaAs Optically-Activated Modulator in Comparison with Existing Active Devices.....2
Table 2 Waveguide Dimensions and Orientations of GaAs/GaAlAs Channel Waveguide Optically Activated Modulator and Modulator Array 9

1.0 INTRODUCTION

The first laser was built in 1960 and within a decade laser beams spanned the range from infrared to ultraviolet. The availability of high power coherent sources led to the discovery of a number of new optical effects (second harmonic generation, linear and quadratic electrooptic effects, etc.) and thus to the development of a myriad of marvelous new devices. The technology needed to produce practical optical communication devices and systems is fast evolving.

The sophisticated use of crystals in devices such as second harmonic generators, electrooptics, acoustooptics, and magneto-optics has spurred a great deal of contemporary research in crystal optics. In the early 1970's, the concept of integrating different passive and active devices, such as lasers, waveguides, modulators, detectors, lenses, and prisms, in hybrid or monolithic forms was introduced. Integrated optoelectronics is a far-reaching attempt to apply thin film and integrated electronics technology to optical circuits and devices. By means of integrated optics, one has the potential to achieve higher speeds and more economical optical communication and data processing systems. Integrated optics can also provide a more convenient interface between optical and electronic systems.

One of the major building blocks of optoelectronic integrated circuits (OEIC) is the optical guided wave modulator. The realization of optical communication and computing with high parallelity, large modulation bandwidth and low propagation loss have made the optical wave an attractive information carrier.

Within the past fifteen years, several types of guided wave electrooptic modulators have been built. The electrooptic modulation of light can be separated into phase [1-5], polarization [6,7], intensity [8-9] modulation, and multi-quantum well (MQW) [10] modulation. The fundamental emphasis of electrooptic and all-optical modulators is focusing on changing the index of refraction of the optical and electrooptic materials within which the optical waves propagate. In this SDIO-sponsored Phase I program, an optically activated modulator on a GaAs/GaAlAs compound semiconductor channel waveguide was proposed and then successfully developed. The devices we report here can be used as optically enhanced phase modulators or as an optically activated cutoff modulators. The device parameters can be designed to satisfy the criterion needed for either case. The principle of operation and the device structure are introduced in Section 2.0 of this report. Design rules for all-optical modulators are detailed as well.

Section 2.0 also includes a description of the fabrication procedure for the proposed device. The etching process, channel waveguide formation on the GaAs/GaAlAs substrate, optical window formation, channel waveguide edge cleavage to facilitate end-fire coupling, and device packaging are reported on. Performance of the modulators and modulator arrays is detailed in Section 3.0. Demonstration of optically activated phase modulators is presented first followed by considerations for waveguide design and the reporting on optically activated modulators working at the cutoff boundary. The phase shift of the guided wave as a function of modulating optical wave (visible) is measured. Index modulation due to optically-generated free carriers has proven to be two orders of magnitude higher than the linear electrooptic effect. Incorporation of a DC-biased voltage enhanced the modulation depth. The theoretically projected modulation speed is provided. The ultimate limitation on the speed of this type of device is the free carrier lifetime of the semiconductor material involved. This is similar to counterpart microwave devices. For undoped GaAs the carrier lifetime is around 10 ns [11]. Carrier lifetime in picosecond to subpicosecond range has been achieved in GaAs by using doping or ion implantation techniques [12,13]. The Phase I results demonstrate that device length (5 μm in the Phase I demonstration) even

shorter than for multiple quantum well devices is enough to provide a high extinction ratio for the optical throughput of the modulator. Depending on the application scenario, both all-optical and electrooptic modulators are realizable. A variety of feasible applications, including optical gates, time division multiplexing, the generation of optical pulses, matrix-matrix multiplication, laser beam incident direction sensors and IR countermeasure systems, are described in Section 4.0. The proposed optically activated GaAs/GaAlAs channel waveguide modulator promises to be very useful for the above mentioned applications. Finally, concluding remarks are made in Section 5.0. Table 1 summarizes the experimentally confirmed flatness of the proposed modulator in comparison with existing devices.

Table 1. Demonstrated Features of the GaAs Optically-Activated Modulator in Comparison with Existing Active Devices

Technology / Parameter	GaAs OAM	$LiNbO_3$ E-O Device	GaAs E-O Device	MQW	Plasmon Modulator	$\chi^{(3)}$ Nonlinear All Optical Device
IR Optical Bandwidth	High	High	High	Very Low	Extremely Low	Low
Power Consumption	Low	High	High	Low	High	Very High
Status of Development	New Concept	Well Developed	Well Developed	Well Developed	Recently Developed	Recently Developed
Extinction Ratio	High	High	High	High	High	High
Interaction Length	Short[a]	Long	Long	Short	Short	Short
Modulator Speed	High[b]	High	High	High	High[c]	High
Reliability	Very Good	Good	Good	Poor	Poor	Poor
Cost	Low	High	High	Very High[d]	High	Very High[e]
Practicality	Very Good	Good	Good	Poor	Poor	Poor
Coherence of Signal Carrier	Not Required[f]	Required	Required	Required	Required	Required

[a] 5 μm interaction length was demonstrated in Phase I.
[b] Only limited by carrier lifetime which can be in the subpicosecond range.
[c] Theoretical prediction.
[d] Needs MBE machine to grow multilayer structure.
[e] Needs high power laser as the activation source.
[f] Both LEDs and LDs can be employed for the OAM working at the cutoff regime.

2.0 PRINCIPLE OF OPERATION AND DEVICE STRUCTURE

The throughput of data and signal processors are being pushed to ever increasing limits. The development of fast, more sophisticated integrated circuits and the use of parallel processing are largely responsible for this improvement. Due to the intrinsic material limitations of silicon, such as small electron and hole mobility (compared to GaAs), indirect band gap, and inability to produce semi-insulating substrates, more and more research has been concentrated on other semiconductor materials which do not have these limitations. In order to provide high data rate communication, multi-gigahertz clock distribution and high packing density of interconnection channels, photons (bosons), instead of electrons (fermions), are taking over the role of signal carriers for many communication systems.

GaAs provides a direct band gap, high electron and hole mobilities, and semi-insulating substrates. The combination of these characteristics allows us to make high speed,

monolithic, optoelectronic integrated circuits. In this program, we propose a new GaAs-GaAlAs heterostructure channel waveguide modulator. Optical waves of any light with wavelengths within the 0.9 to 5 μm range can be used as the signal carrier. Optical photons from both coherent and incoherent light sources with $h\nu > E_g$ (i.e., energy gap of GaAs waveguides) can be employed as the source for activating a vast number of free electrons and holes. The basic structure for the single-channel optically-activated modulator (OAM) on a GaAs-GaAlAs waveguide is shown in Figure 1. The small circular window area between the two electrode pads is designed to input the optical photons with $h\nu > E_g$ to generate free electron and hole pairs. The optical wave representing the signal carrier can be coupled into the waveguide through end-firing or by a grating. A reverse bias can be added across the Schottky barrier to form a depletion region to accelerate the free carriers.

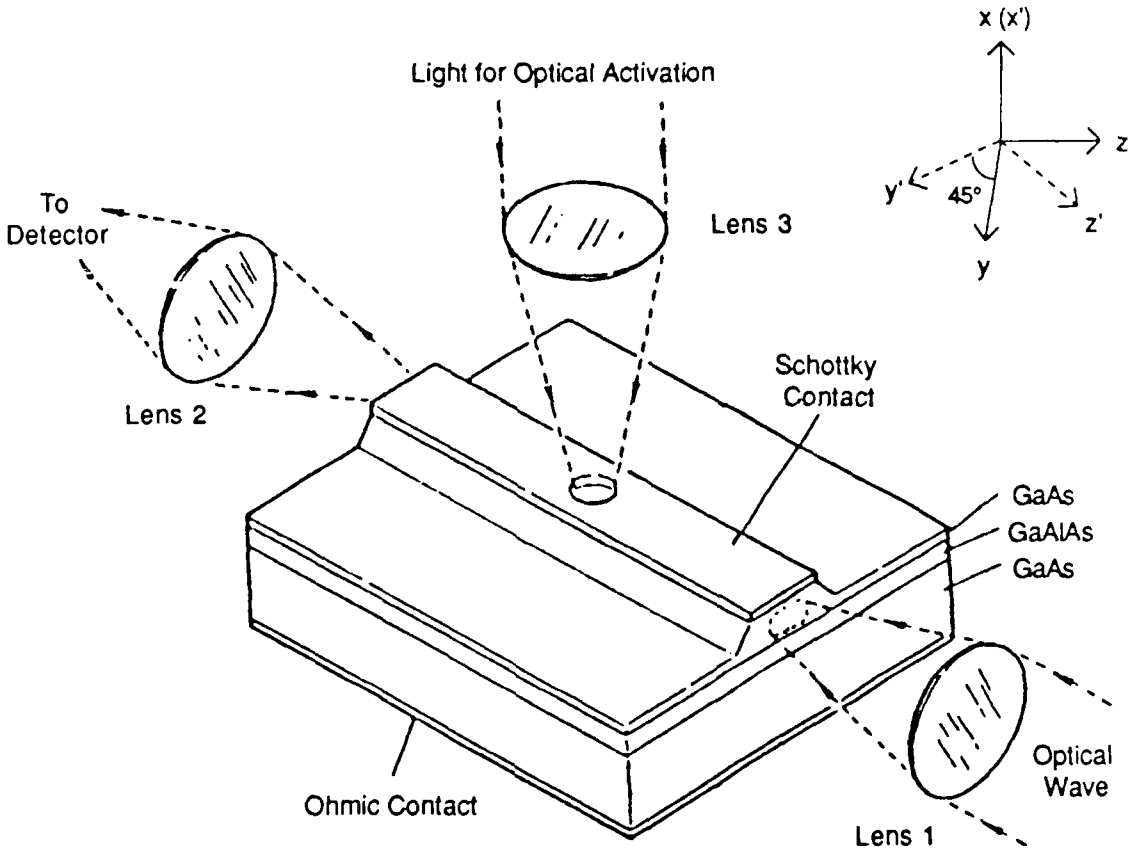

Figure 1
Basic Structure of Optically Activated Modulator on GaAs

2.1 The Working Principle

A discussion of the working principle of the modulator follows. A very large index change induced by current has been reported on Si [14, 15], GaAs-GaAlAs [16-18], and InGaAsP-InP [19,20]. Since the current induced index change is much stronger than the linear electro-optic effect, we can make an active device by injecting a time dependent

carrier concentration. The current is first induced by shining strong condensed light, with photon energy larger than the band gap of the guiding layer material, on the window area shown in Figure 1. A very large current density is induced in this way. When the optical signal carrier to be modulated is coupled to the ridge waveguide, the induced current will interact with the guided wave. The equation of motion of an electron in an electric field E_y of frequency $\omega/2\pi$ (frequency of light to be modulated) along the vector direction of the electric field, say y, is

$$m_e^* \frac{dv_y}{dt} = -e \cdot E_y = -e \cdot E \cdot e^{i\omega t} \tag{1}$$

where m_e^* is the effective mass of an electron and E_y is the electric field of the optical carrier. The solution for Eq. (1) is

$$V_y = V_{yo} + \frac{ie \cdot E}{\omega \cdot m_e^*} e^{i\omega t} \tag{2}$$

Since the mean velocity without the influence of E_y is 0, the first term V_{yo} is zero also. The current induced by this optical field (not the current across the junction) is

$$J_y = N \cdot e \cdot V_y = \frac{iN \cdot e^2 \cdot E}{\omega \cdot m_e^*} e^{i\omega t} \tag{3}$$

The current density induced by an electric field can also be written as

$$J_y = \sigma \cdot E_y \tag{4}$$

where σ is the conductivity. Combining Eqs. (3) and (4), we have

$$\sigma = \frac{iN \cdot e^2}{\omega \cdot m_e^*} \tag{5}$$

The dielectric constant and conductivity enter into a determination of the optical properties of a solid only in the combination [21]:

$$\varepsilon(\omega) = n_o^2 + \frac{4\pi i\sigma(\omega)}{\omega} \tag{6}$$

where n_o is the index of refraction without the influence of current. From Eq. (5), we can easily write Eq. (6) in the following form:

$$\varepsilon(\omega) = n_o^2 - \frac{4\pi Ne^2}{m_e^* \omega^2} \tag{7}$$

Since the value of the second term in Eq. (7) is much less than n_o^2, the index of refraction can be written in the following approximate form:

$$n = (\varepsilon)^{1/2} \cong n_o \cdot \left(1 - \frac{2\pi Ne^2}{m_e^* \omega^2 n_o^2}\right) \tag{8}$$

The Δn value in this condition is

$$\Delta n = \frac{-2\pi N e^2}{m_e^* \omega^2 n_o} \tag{9}$$

Since both electrons and holes contribute to the current, Eq. (9) can be written as

$$\Delta n = \frac{-2\pi N_e e^2}{m_e^* \omega^2 n_o} + \frac{-2\pi N_p e^2}{m_p^* \omega^2 n_o} \tag{10}$$

where N_e and N_p represent the concentration of electrons and holes, respectively. By using the Kramers-Kronig relations, the absorption associated with free electrons and free holes is [14]:

$$\Delta\alpha = \left(e^3\lambda^2/4\pi^2C^3\varepsilon_o n_o\right)\left[N_e/m_o^{*2}\mu_e + N_h/m_p^{*2}\mu_p\right] \tag{11}$$

where e is the electron charge ε_o is the permittivity of free space, μ_e is the electron mobility, and μ_p is the hole mobility. With the interaction length we proposed (5 μm), the throughput intensity modulation is mainly due to refractive index modulation (Eq. (10)) rather than absorption (Eq. (11)) [22]. It has been proven in the Phase I tasks that the change of index of refraction due to the injected free carriers can be two orders of magnitude higher than that generated by the linear electro-optic effect. A device interaction length compatible with multi-quantum well structure is achievable using the proposed concept.

Another important conclusion from Eq. (10) is that in contrast to the linear electro-optic effect, which depends upon the vector electric field, the induced index change is a scalar function. If the effective masses of electrons and holes in the two different transverse directions are the same, then the induced change of the guiding layer index is the same for both TE and TM guided waves. This eases the requirement needed for the direction of waveguide propagation.

As shown in Figure 1, a Schottky contact is built on top of the channel waveguide. The reverse bias field added across the Schottky barrier is to increase photon generated electron-hole pairs (EHPs) within a diffusion length of the transition region in the semiconductor. The lack of free carriers within the space charge transition region can create a current due to the net generation of carriers by emission from recombination centers [23] and valence band-to-conduction band transition. The I-V characteristic of the fabricated device will be described in Section 4.0.

It is clear from the discussion above that an optically activated modulator does not depend on the orientation of the GaAs crystal. The free-carrier induced index modulation reduces the effective index of the guided mode isotropically The device structure presented in the next section allows experimental observation of the magnitude of the current-induced index modulation to be compared with the magnitude of the linear electrooptic effect.

2.2 Device Structure for Comparison All-Optical and Linear E-O Effects

To quantitatively compare the magnitude of the index modulation due to optical activation and to the linear electrooptic effect, an optical modulator that can work on both mechanisms needs to be built. For OAM crystal orientation is not an influential factor. However, for GaAs a cubic crystal which belongs to the symmetry group $\bar{4}3$ m, the EO effect does depend on the orientation of the crystal. The EO tensor of GaAs may be written in the following form:

$$r_{ij} = \begin{pmatrix} 0 & 0 & 0 \\ 0 & 0 & 0 \\ 0 & 0 & 0 \\ r_{41} & 0 & 0 \\ 0 & r_{41} & 0 \\ 0 & 0 & r_{41} \end{pmatrix} \tag{12}$$

The only nonvanishing elements are $r_{41} = r_{52} = r_{63}$. The index ellipsoid in the presence of a modulating electric field $\vec{E}\left(E_x, E_y, E_z\right)$ can be represented by the following quadratic equation:

$$\frac{x^2}{n_o^2} + \frac{y^2}{n_o^2} + \frac{z^2}{n_o^2} + 2r_{41}E_x yz + 2r_{41}E_y xz + 2r_{41}E_z xy = 1 \tag{13}$$

where the constants involved in the first three terms do not depend on the modulating field and, since the crystal is cubic, are designated as $n_x = n_y = n_z = n_o$. Thus, application of an electric field generates cross terms in the quadratic equation. For the device configuration shown in Figure 1, since the electric field is applied along the x-axis, Eq. (13) becomes

$$\frac{x^2 + y^2 + z^2}{n_o^2} + 2r_{41}E_x yz = 1 . \tag{14}$$

The task at hand is to find a new coordinate system (x',y',z') in which the equation of the index ellipsoid, Eq. (13), contains no mixed terms; that is, it is of the form

$$\frac{x'^2}{n_{x'}^2} + \frac{y'^2}{n_{y'}^2} + \frac{z'^2}{n_{z'}^2} = 1 \tag{15}$$

where x', y', and z' are then the major axes of the index ellipsoid in the presence of an external field applied along (100).

In the case of Eq. (14), it is clear that in order to eliminate the cross term we need to choose a coordinate system x', y', z', where x' is parallel to x. Because of the symmetry of

Eq. (14) in y and z, the coordinates y' and z' are related to y and z by a 45° rotation as shown in Figure 2. The transformation relations from y, x to y', z' are thus

$$y = y' \cos 45° - z' \sin 45° \tag{16}$$

$$z = y' \sin 45° + z' \cos 45° \tag{17}$$

which, upon substitution in Eq. (14), yields

$$\left(\frac{1}{n_o^2} + r_{41}E_x\right)y'^2 + \left(\frac{1}{n_o^2} - r_{41}E_x\right)z'^2 + \frac{x^2}{n_o^2} = 1 \tag{18}$$

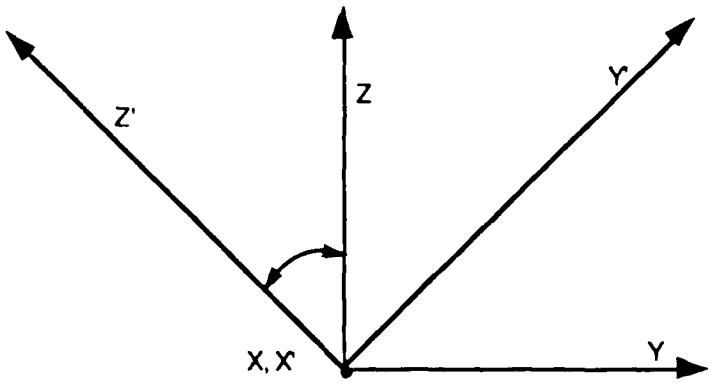

Figure 2
Rotation of Principal Axes of GaAs Due to the Existence of an Electric Field

This equation shows that x, y', and z' are indeed the principal axes of the index ellipsoid when a field is applied along the x-direction. We also see that the length of the y' axis of the ellipsoid is $n_{y'}$, where

$$\frac{1}{n_{y'}^2} = \frac{1}{n_o^2} + r_{41}E_x \,. \tag{19}$$

Since in practice $r_{41} << n_o^2$, the following Taylor expansion is valid

$$\left(1 + r_{41}E_x n_o^2\right)^{-1/2} \approx 1 - r_{41}E_x n_o^2/2 \,. \tag{20}$$

Thus

$$n_{y'} = n_o - n_o^3 r_{41}/2 \,. \tag{21}$$

Similarly,

$$n_z' = n_o + n_o^3 r_{41}/2 . \quad (22)$$

Finally,

$$n_x' = n_o . \quad (23)$$

Eq. (18) shows that a rotation of 45° for the principal axes in the y-z plane results when an electric field is applied along the [100] direction in the basic cutoff modulator as shown in Figure 1. It is to be noted that the ridge channel waveguide is oriented along the [011] on (100) plane. We designed this structure to measure the magnitude of the index modulation due to the generation of free carriers in comparison with the modulation due to the well-known linear E-O effect. Note that the optically activated modulator working in both phase- and cutoff-modulation regimes can be realized on any orientation of GaAs crystal.

2.3 Device Fabrication

A single-mode optically-activated modulator and a linear array of identical modulators have been successfully fabricated. First, a planar GaAs-GaAlAs heterostructure with an aluminum concentration of approximately 7% was grown on an x-cut N^+ substrate using a MOCVD system [24]. Planar waveguide formation was first confirmed experimentally through end-fire coupling. The channel waveguide and waveguide array were made through the conventional lithographic process. AZ1400 photoresist was employed as the masking material during the wet etching process which consisted of HCl, H_2O_2, and H_2O in the ratio of 80:4:1, and provided an etching rate of 1.1 μm/min at room temperature. After the channel waveguide was empirically verified to be a successful optical guide, a thin Al film was deposited on the waveguide surface. A lift-off technique was employed to form the desired window for optical activation. A circular window 5 μm in diameter was formed on top of the channel waveguide. The microstructure revealed by a high resolution microscope is shown in Figure 3. The channel waveguide, Al electrode and the 5 μm diameter window are clearly displayed. The parameters and waveguide orientations for both the basic modulator and the modulator array are given in Table 2. Finally, after formation of an ohmic contact on the bottom face of the specimen, both end faces of the device were cleaned to facilitate edge coupling for subsequent experiments. Figure 4 shows the photograph of one of the cleaved end faces of the modulator array. The finished sample was then mounted on a special IC chip and placed in a device holder for detailed experimentation. The device package is shown in Figure 5. Bonding wires, chip carrier, GaAs OAM, 50 Ω microstrip line and SMA connectors are clearly shown.

Table 2. Waveguide Dimensions and Orientations of GaAs/GaAlAs Channel Waveguide Optically Activated Modulator and Modulator Array

Common Parameters:	
Channel Width	5 μm
Channel Depth	1 to 1.5 μm
Waveguide Type	Ridge Channel
Etching Solution	$HCl:H_2O_2:H_2O = 80:4:1$
GaAlAs Thickness	1 μm
Al Concentration	7 percent
Schottky Contact	Al 5000 Å thick
Substrate Orientation	(100)
Waveguide Direction	[011]
Window Size (Interaction Length)	5 μm in diameter
Cutoff Modulator Array:	
Separation Between Adjacent Channels	20 μm
Area of Bonding Pad	4 mil. x 4 mil.
No. of Channels	10
Packing Density	500 channels/cm

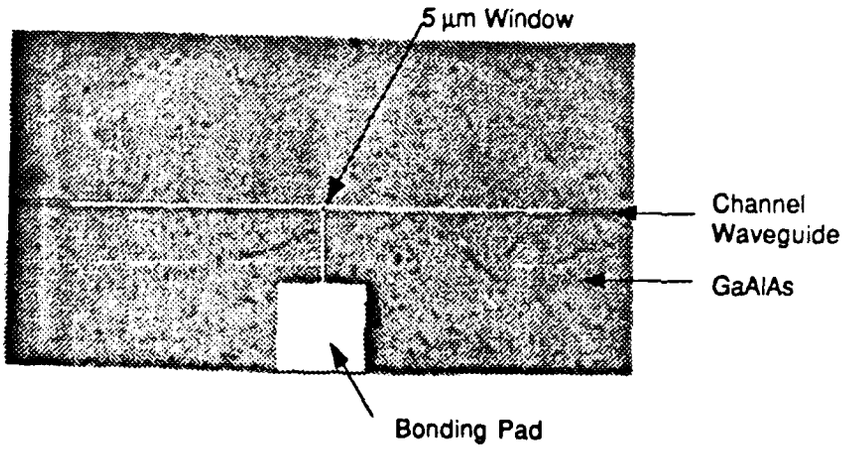

Figure 3
0.5 mm Electrode on a GaAs/GaAlAs Channel Waveguide and 5 μm Diameter Window for Optical Activation on a Single-Mode GaAs/GaAlAs Channel Waveguide

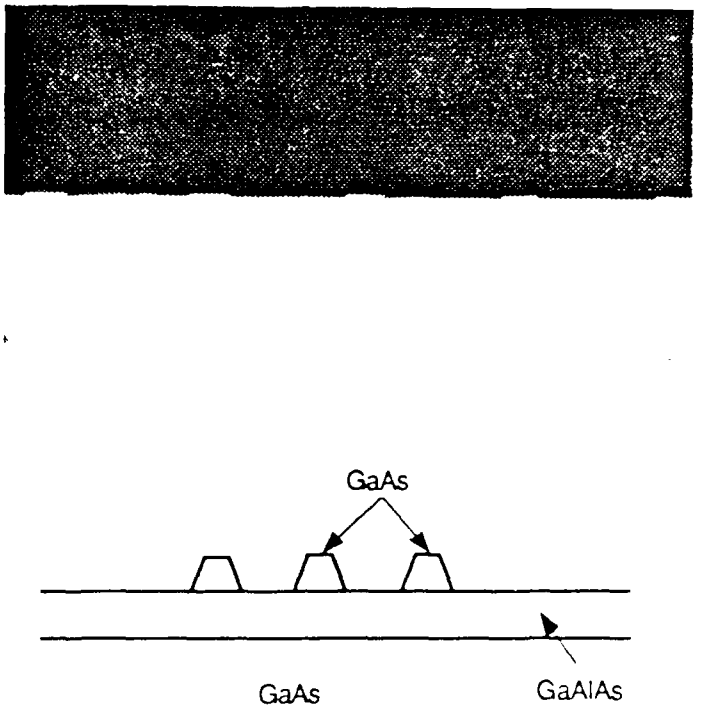

Figure 4
Illustration of One of the Cleaved End Faces of the Modulator Array

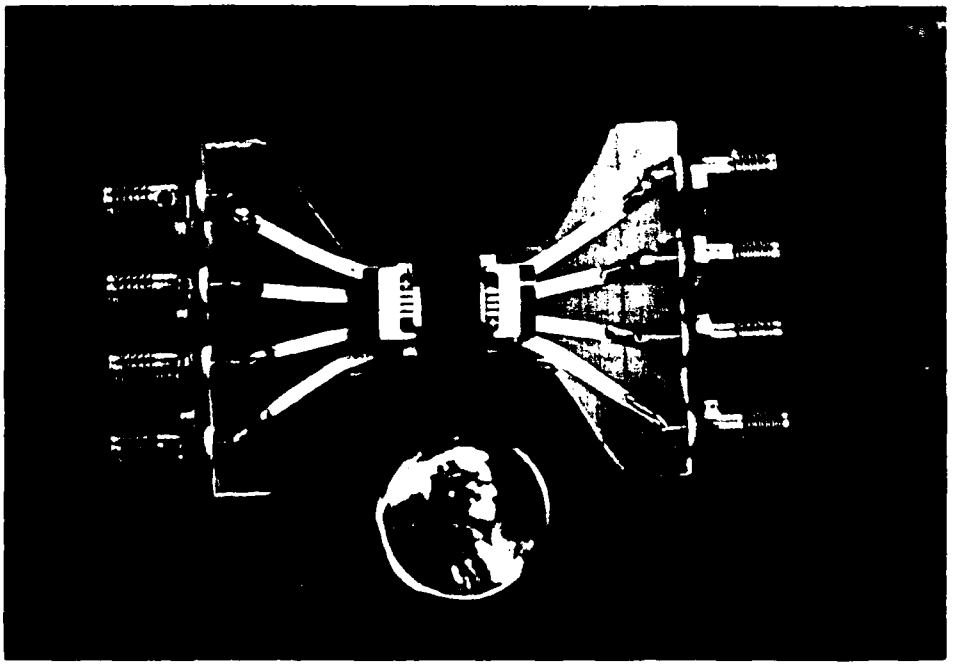

Figure 5
Fully Packaged Optically-Activated Modulator (OAM) on
GaAs-GaAlAs Channel Waveguide

3.0 PERFORMANCE OF THE MODULATOR AND THE MODULATOR ARRAY

In this section, the Phase I experimental results are presented. The setup employed to do the all-optical and the electrooptic measurement is described first. An optically-activated modulator working in the phase modulator regime (well above the cutoff boundary) was produced. The feasibility of using the same device with a 0.5 mm electrode (Figure 3) as a linear electrooptic modulator is also introduced. Theoretical calculation was conducted using the confinement factor as an indicator to determine device criterion suitable for either the phase- or cutoff-regime. The result of the calculation is summarized in Section 3.3. Further results of the optically activated and electrooptic cutoff modulator is reported in Section 3.4.

Conclusions based on experimental results are that (1) a device interaction length (5 μm in the Phase I demonstration) shorter than that of MQW's is capable of generating a 33% modulation depth by using optical activation, (2) optical activation produces an index modulation two orders of magnitude larger than does the linear electrooptic effect (r_{41} in the case of GaAs), and (3) both all optical and electrooptic modulators were proven to be feasible.

3.1 Experimental Setup

The setup employed for the Phase I demonstration is shown in Figure 6 where the optical activation source (0.632 μm HeNe), 1.3 μm laser diode, GaAs/GaAlAs channel waveguide modulator package, coupling and imaging lenses, Ge photodetector (PIN) and the signal generator are clearly shown. A key portion of the setup is detailed in Figure 7 where the area of interaction is clearly indicated. The window area is located right on top of the GaAs channel waveguide within which the 1.3 μm laser light is propagating. The optical activation source can be introduced by using either an imaging lens (Figure 1) or a single-mode fiber (not shown). The coupling lens (Figure 6) provides a diffraction-limited beam waist at the input edge of the waveguide OAM. The imaging lens transfers the near field image of the throughput light from the channel waveguide to the detector. A near field image of the guided wave (1.3 μm) taken by a vidicon camera is illustrated in Figure 8. The background noise was filtered out after the Fourier transform lens. Modulation of the device is observed through the oscilloscope.

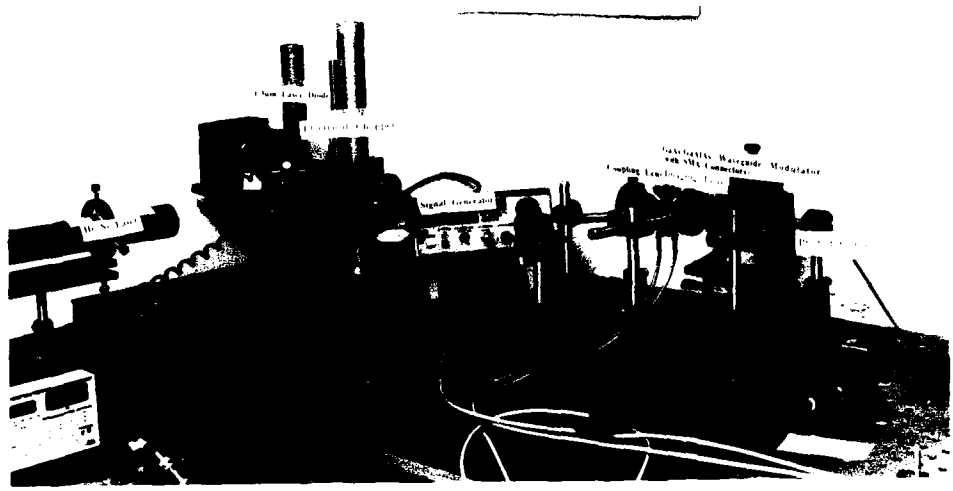

Figure 6
Setup for OAM on GaAs/GaAlAs Channel Waveguide

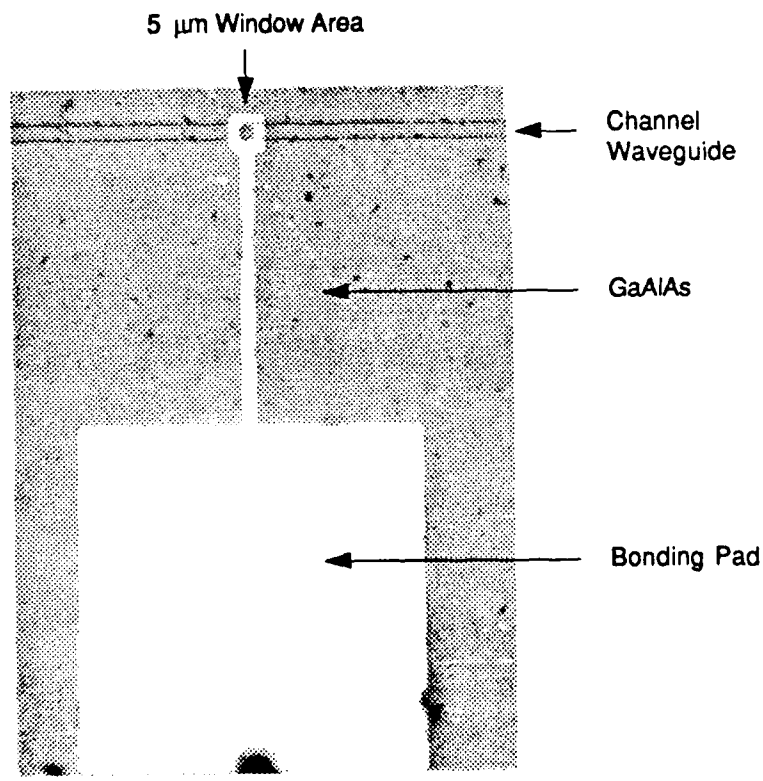

Figure 7
Photograph of the Window for Optical Activation (5 μm in Diameter)

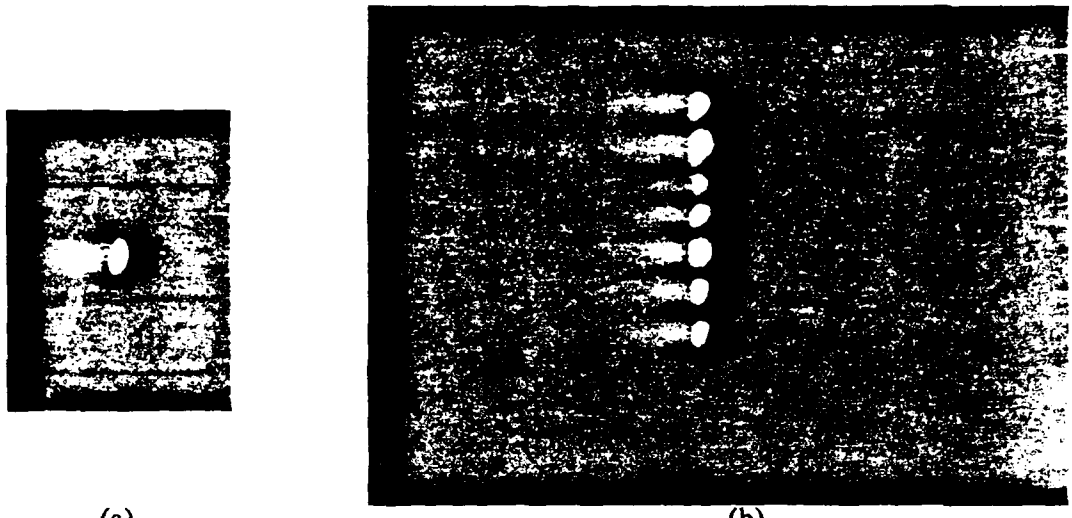

(a) (b)

Figure 8
Near-Field Pattern of the Single-Mode Guided Wave from GaAs/GaAlAs Channel Waveguide. (a) Single-Channel and (b) Channel Waveguide Array.

3.2 Optically Activated Phase Modulator

The first device we demonstrated was a single-mode optically activated phase modulator. By shining the HeNe 0.632 μm on the 5 μm diameter window area, we generated a 33% modulation depth. An index modulation on the order of 10^{-2} was experimentally determined. The results we demonstrated in Phase I provide us with not only a new GaAs waveguide device but also a device interaction length compatible or even shorter than that of MQW devices (~100 μm).

For a Fabry-Perot phase modulator, the percentage of the optical wave transmitted through the output end face of the channel waveguide is given by

$$T = \frac{I_t}{I_i} = \frac{(1 - R)^2 \cdot L}{(1 - RL)^2 + 4RL \sin^2(\delta/2)} \tag{24}$$

where I_t and I_i are the intensity of transmitted and incident lights, respectively, R is the reflectance of the waveguide end faces, L is the propagation loss of the guided wave per round trip and

$$\delta = \frac{4\pi n_{eff} \cdot d}{\lambda} \tag{25}$$

for the guided wave. In Eq. (25), n_{eff}, d, and λ are, respectively, the effective index of the guided mode, the cavity length and the optical wavelength (1.3 μm in the Phase I demonstration). The maximum transmission occurs when

$$\delta = n\pi, \qquad n = \text{any integer} \tag{26}$$

The maximum transmission according to Eq. (24) can be represented by

$$T = \left(\frac{I_t}{I_i}\right)_{max} = \frac{(1 - R)^2 \cdot L}{(1 - RL)^2} . \qquad (27)$$

The existence of loss reduces the peak transmission to less than unity. Figure 9 shows the curves of I_t/I_i with different propagation loss as a parameter. The reflectance R is set at 30%, which is the case at the GaAs/air interface. It is clear that to increase the device modulation depth, the GaAs/GaAlAs waveguide propagation loss should be reduced to a minimum value. From Eqs. (24) and (25), it is obvious that the effective index modulation, i.e., Δn_{eff}, due to optical activation can be found by measuring the T value. The optically activated modulation is shown in Figure 10. The top trace is the HeNe 0.633 μm modulating light source and the bottom trace the modulated guided wave (1.3 μm) which was end-fire coupled into the channel waveguide. Modulation depth to 33% was observed for a waveguide with 0.4 dB/cm propagation loss. It is clear that in order to increase the throughput intensity, waveguide propagation loss needs to be minimized. Figure 11 shows the measured phase shift as a function of the intensity of the optical activation. Index modulation as high as 10^{-2} has been observed. This is two orders of magnitude higher than the linear electrooptic effect. To compare the optically activated modulation with a linear electrooptic phase modulator, an AC electrical field was added to the electrode. The experimental results in Figure 12 show that in order to generate the same T value (33% in this case), we need to have a linear electrooptic device with 1 mm interaction length and 10 volt applied voltage. The interaction length is 200 times longer than the linear dimension of the window of the optically activated modulator. Such compactness significantly enhances the packing density of the modulator array. Note that the modulation depth of 33% corresponds to ~55° phase shift. If the optical window is enlarged to 15 μm, the maximum value of T will be generated.

There are three sources of modulation which can be used in the waveguide modulator. They are: 1) direct modulation of the 1.3 μm laser diode by varying the current of the laser diode driver, 2) optical activation using the 0.632 μm HeNe laser, and 3) electrical signal applied directly onto the Schottky contact located on top of the channel waveguide (Figure 7). Combinations of these modulation mechanisms were tried and the results are shown in Figure 13. Note that the combination of these modulation outputs is shown as the bottom trace of the photograph. An array of useful applications is implied by this figure. Time division multiplexing and optical gates are some of the most promising ones. The details of these applications will be described in Section 4.0.

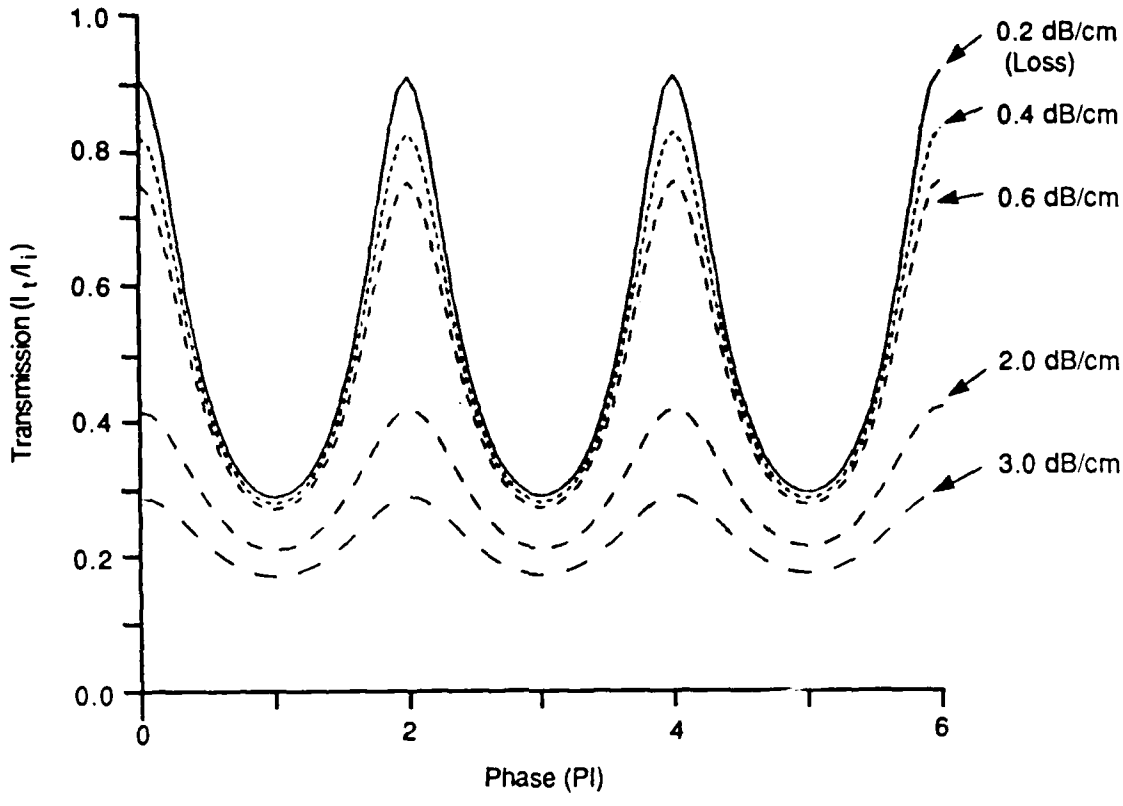

Figure 9
Transmission (I_t/I_i) of the GaAs OAM as a Function of Phase Shift with Waveguide Propagation Loss as a Parameter

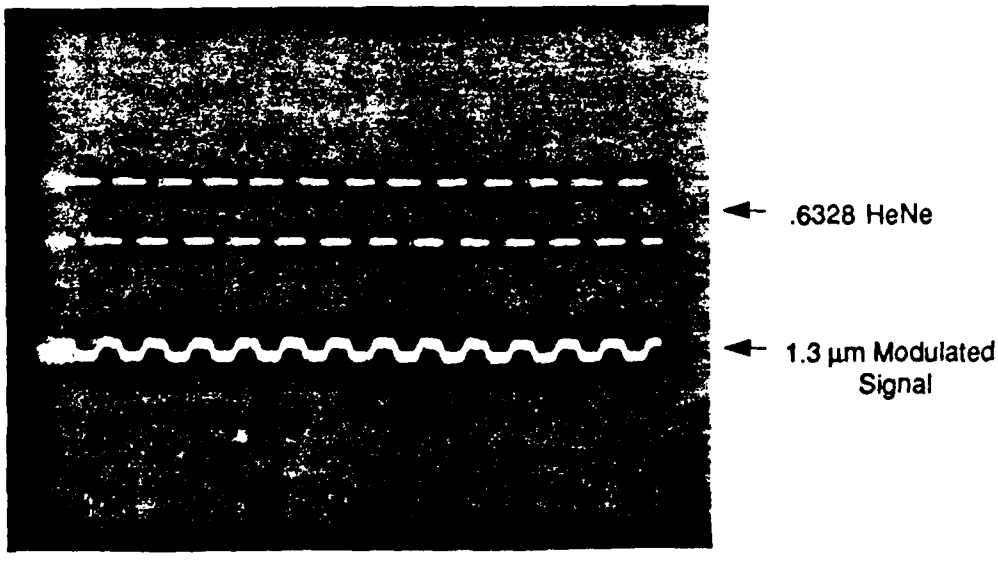

Figure 10
Optically Activated Modulator: Top Trace = 0.633 µm Modulating Light Source, Bottom Trace: Modulated 1.3 µm Guided Wave (Modulation Speed 4 kHz)

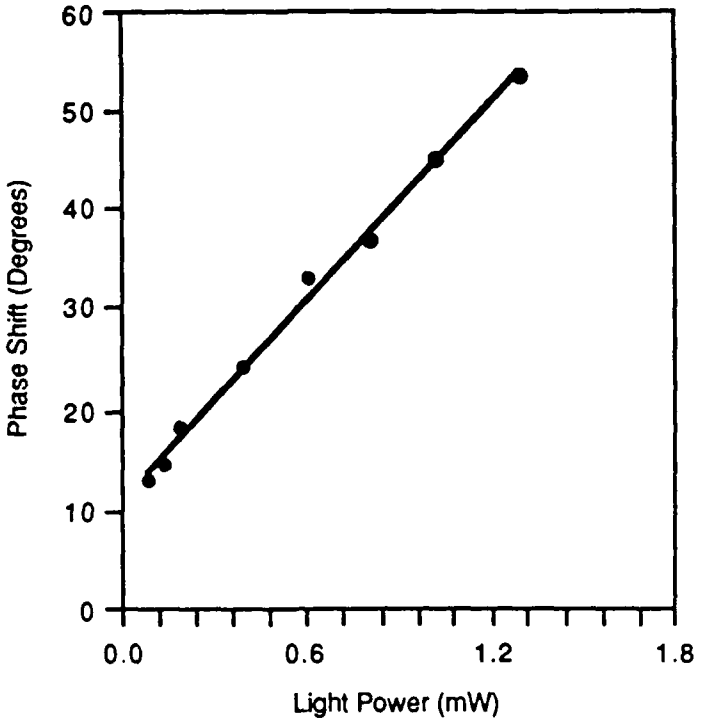

Figure 11
Photo-Induced Phase Shift in the Guided Light Versus Modulating Light Power with Interaction Length of 5 μm

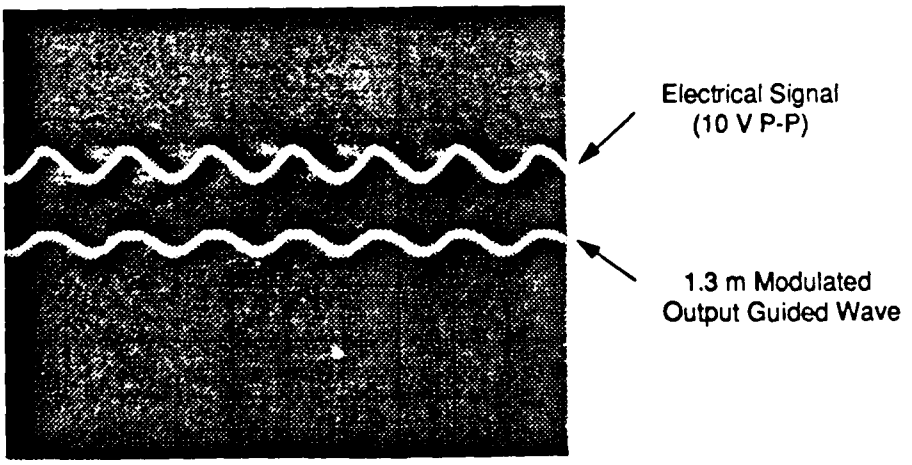

Figure 12
33% Modulation Depth of the 1.3 μm Guided Wave Throughput Generated Directly from a 0.5 mm Electrode with 10 Volt Peak to Peak Value at 4 kHz

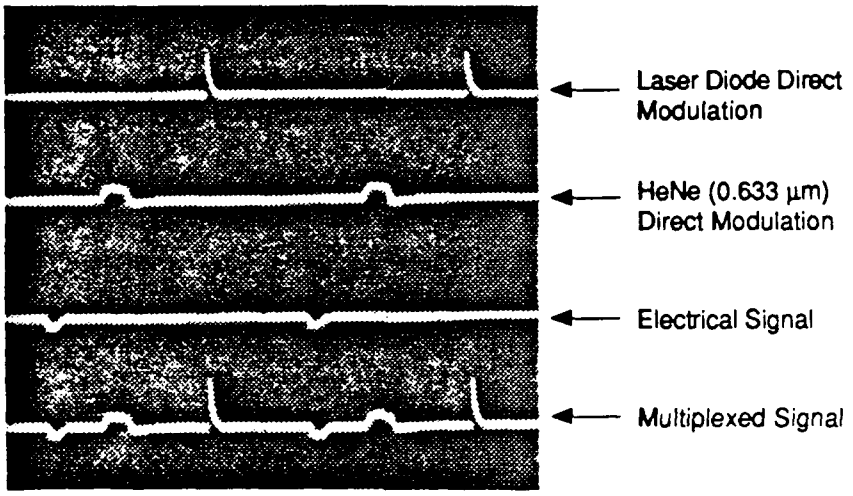

Figure 13
Detection of the 1.3 μm Output Signal from the GaAs Channel Waveguide. Multiplexing of These Three Signals are Shown. The Modulation Frequency is Fixed at 4 kHz.

3.3 Waveguide Design Considerations

Experimental results we observed show that the optically activated modulator (OAM) can work either as a Fabry-Perot phase modulator or a cutoff modulator. Both the phase modulator and the cutoff modulator are single-mode devices which use the same electrode structure. The difference between them is that the optically activated phase modulator is well above the cutoff so that the confinement factor C_f, which is defined as

$$C_f = \frac{|\langle W|W\rangle|_{\text{guiding region}}}{|\langle W|W\rangle|_{\text{guiding region}} + |\langle W|W\rangle|_{\text{cladding regions}}}, \qquad (28)$$

is not changed significantly by the existence of an external bias field. In Eq. (28), $|W\rangle$ is the electric field distribution function of the guided mode. In the case of an optically activated modulator working in the cutoff regime, however, the confinement factor changes drastically. The sensitivity of the waveguide confinement factor C_f to the existence of an applied electric field is a major parameter in determining the waveguide's suitability for use as either an optically activated phase or an optically activated cutoff modulator.

In order to clarify this statement, a theoretical calculation was made to evaluate the influence of the waveguide's effective index on the confinement factor. The experimental results imply that a good optically activated cutoff modulator is achieved by a waveguide with effective index very close to the substrate index. Therefore, it is essential that the waveguide effective index be in the neighborhood of the cutoff boundary. The small variation of the effective index can be induced by either an external voltage or a small

perturbation of such waveguide parameters as aluminum concentration or waveguide dimension.

The channel waveguide used in Phase I was the subject of calculation. It was found that only the evanescent tail penetrating into the GaAlAs cladding layer was changed significantly. A three-dimensional surface plot with effective index as the x-axis, the distance of the waveguide in the depth direction as the y-axis (origin at the center of the GaAs guiding layer), and the electric field of the guided mode as the z-axis, is shown in Figure 13. The refractive index of $Ga_{0.93}Al_{0.07}As$ is 3.3710 at 1.3 μm. The waveguide depth is varied in the neighborhood of 1 μm. The theoretical calculation shows that, when the effective index is very close to 3.3710, the evanescent tail of the guided wave penetrating into the $Ga_{0.93}Al_{0.07}As$ cladding layer is the major reason for the decrease of the confinement factor. The peak of the electric field clearly decreases as the guided mode index moves closer to the cutoff boundary. Each of the waveguide propagating mode profiles shown in Figure 14 is normalized so that

$$\left| \langle W | W \rangle \right| = 1 \tag{29}$$

where $|W\rangle$ is the waveguide mode function and the integration covers all of the area. The equal electric field lines of the various propagating modes corresponding to Figure 14 are shown in Figure 15. The increase of the intensity of the evanescent tail as the effective index of the guided mode moves closer to 3.3710 is clearly shown in this figure. The resulting confinement factor, as defined by Eq. (28), is a function of the guided wave mode index, as shown in Figure 16. The confinement factor drops to zero as N_{eff} shifts to the value of the cladding index. Two regions are evident in Figures 14 and 16. The first region represents the waveguide domain suitable for the optically activated cutoff modulator where the confinement factor changes drastically as a function of the effective index, N_{eff}. The second region is the waveguide domain, suitable for an optically activated phase modulator, where the confinement factor changes slightly under the influence of an external activation source. It is clearly shown in these figures that the dynamic range of the waveguide effective index appropriate for an optically activated phase modulator is larger than that of an optically activated cutoff modulator.

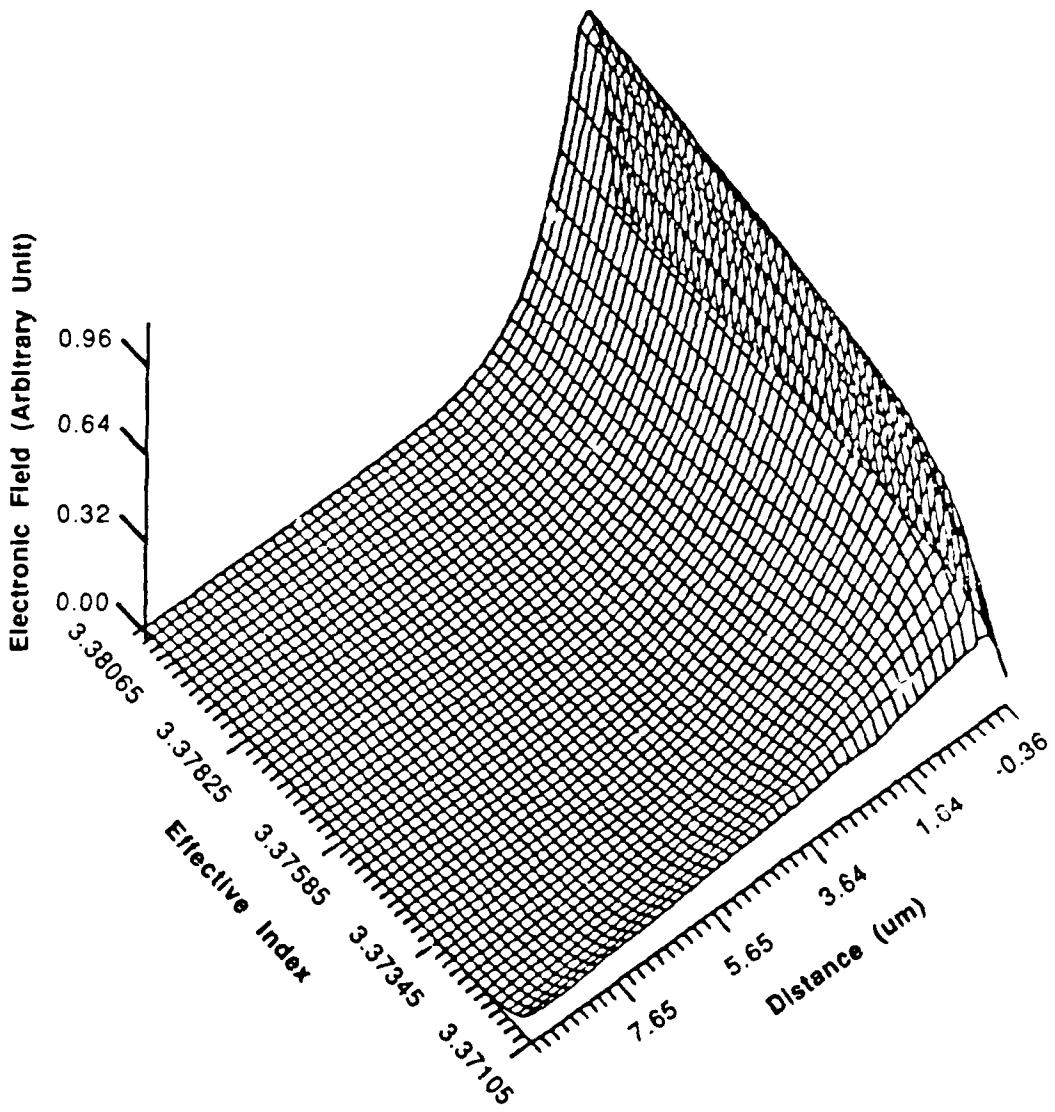

Figure 14
Propagating Mode Profiles Along the Transverse Direction of the GaAs Waveguide (GaAs-$Ga_{0.93}Al_{0.07}As$). The Increase of the Evanescent Wave is Clearly Seen.

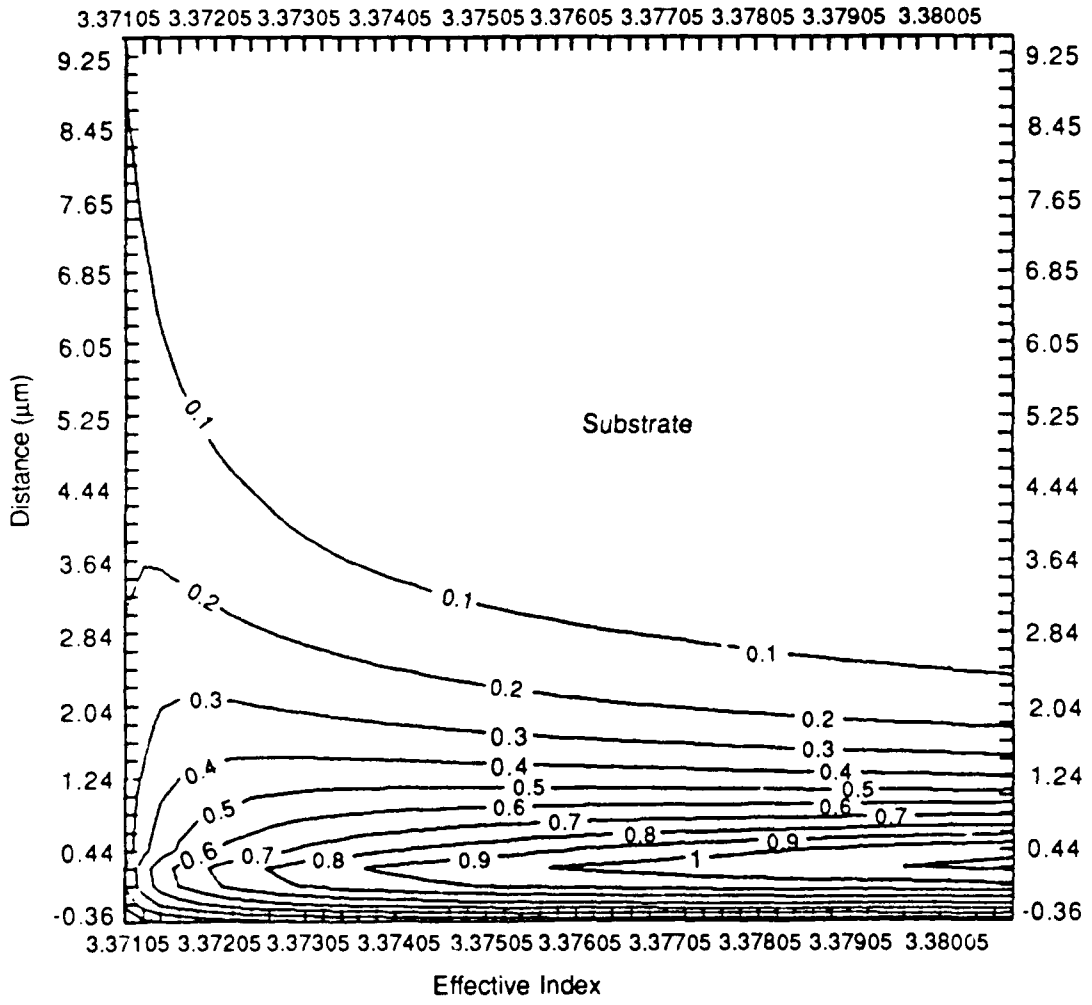

Figure 15
Equal Electrical Field Topology of the Propagating Modes of the GaAs Waveguide (GaAs-$Ga_{0.93}Al_{0.07}As$) Corresponding to Figure 14

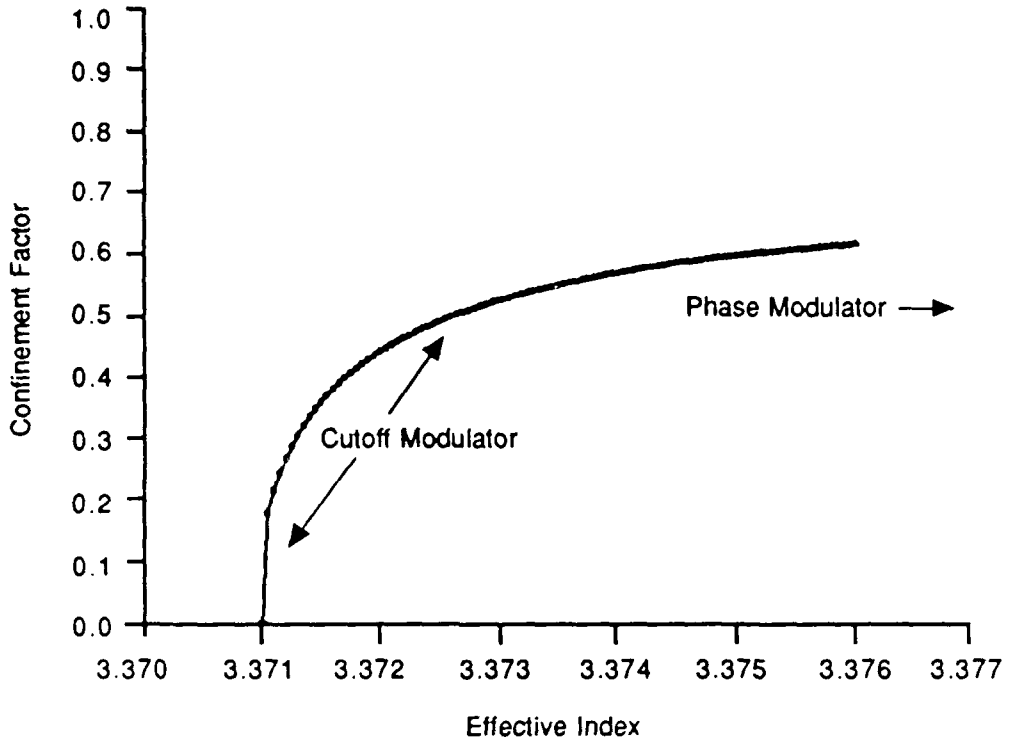

Figure 16
Confinement Factors as a Function of Effective Indices of the GaAs Waveguide
($GaAs\text{-}Ga_{0.93}Al_{0.07}As$)

3.4 Optically Activated Cutoff Modulator

Based on the discussion presented in Section 3.3, a single-mode GaAs-GaAlAs channel waveguide with an effective index closer to the cutoff boundary was tested. The device we tested in this section has a narrower waveguide dimension and is thus closer to the cutoff boundary (Figure 16). The rest of the setup is the same as that shown in Figure 6. Operation of the device can be carried out either by shining DC HeNe laser light on the window area and applying the AC signal through the SMA injection port (Figure 5) or by directly encoding the modulated signal onto the HeNe laser. Figure 17 shows the optically activated modulation by directly modulating the HeNe laser with an electrical chopper. The top trace of the figure is the HeNe laser light and the bottom trace the IR throughput from the GaAs channel waveguide. A modulation depth of 8.5 dB was measured. Note that the device was biased at -12 volts. The existence of a DC bias voltage significantly enhanced the current effect. The induced current under different light intensities were measured first with a curve tracer. The result is shown in Figure 18. The characteristics of a Schottky diode I-V under 0 mW, 0.6 mW, 1.2 mW, 1.8 mW, and 2.5 mW HeNe 0.6333 μm illumination are shown. For a fixed optical activation level, the current density increases proportionally as the reversely biased voltage increases. Note that the modulation depth of the optically activated cutoff modulation was significantly enhanced. The amplification of the IR modulated light as a function of the reverse bias-voltage with a 2.5 mW 0.633 μm

laser shining on the window (Figure 7) of the waveguide surface is illustrated in Figure 19. A total gain of ~13 dB was observed. The intensification of the AC current effect due to the existence of DC bias was experimentally confirmed by shining a chopped HeNe light on the window area while observing the shift of the I-V characteristic curve. The results shown in Figure 20 illustrate the augmentation of the dynamic range of the current swing and thus of the refractive index modulation. The double traces shown in this photograph were due to the scanning of the I-V curve tracer. Our experiment showed that the enhancement of current and index modulation by the HeNe light is much more significant than that of the reverse bias-voltage. The comparison of these two cases, i.e., with and without optical activation, are illustrated in Figure 21. Finally, the modulated output for both TE (transverse electric) and TM (transverse magnetic) modes with and without optical activation are shown in Figure 22. Be aware of the fact that for the crystal orientation of the device shown in Figure 1 the TM mode does not have any electrooptic effect. However, optical activation through current modulation is not polarization-dependent. As a result, both TE and TM modes demonstrated a large magnification of the IR guided wave throughput signal.

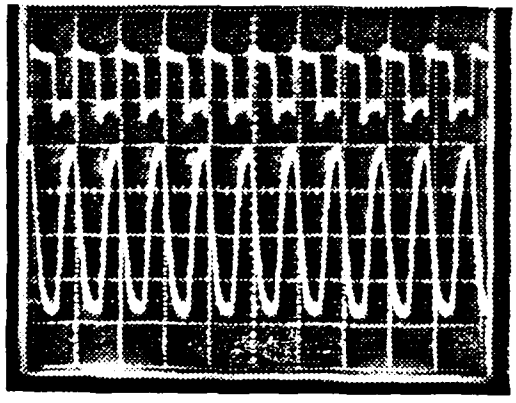

Figure 17
Optically Activated Modulation (Bottom Trace) by Pulsing the Activation Light (Top Trace). Modulation Frequency 4 kHz.

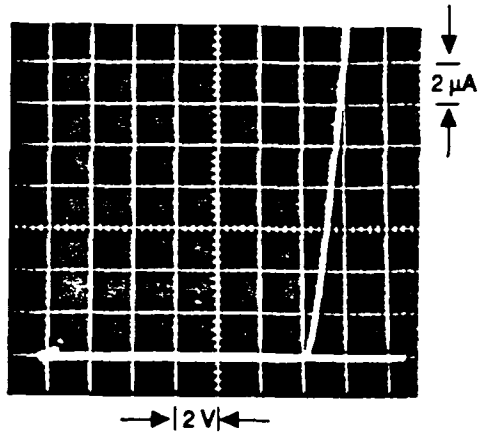

(a)

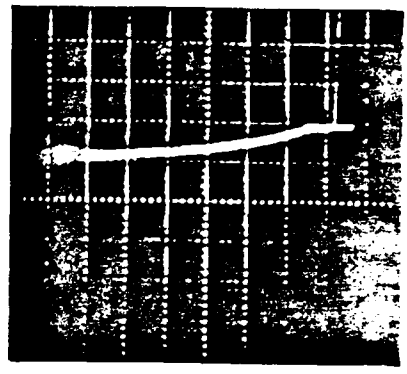

(b)

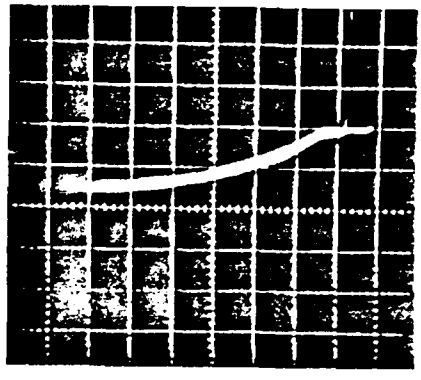

(c)

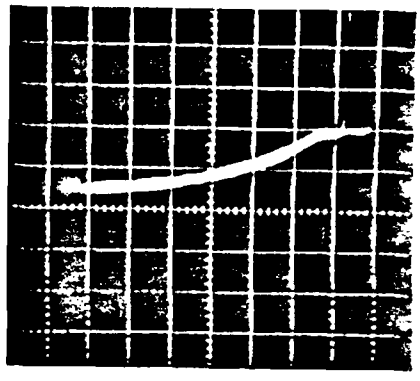

(d)

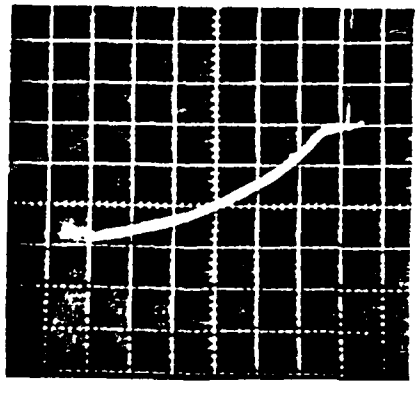

(e)

Figure 18
I-V Curve of the Schottky Diode: (a) Without HeNe 0.6328 μm Light, (b) With 0.6 mW HeNe Light, (c) With 1.2 mW, (d) With 1.8 mW, and (e) With 2.4 mW HeNe Light Shining on the Window Area of the GaAs/GaAlAs Channel Waveguide

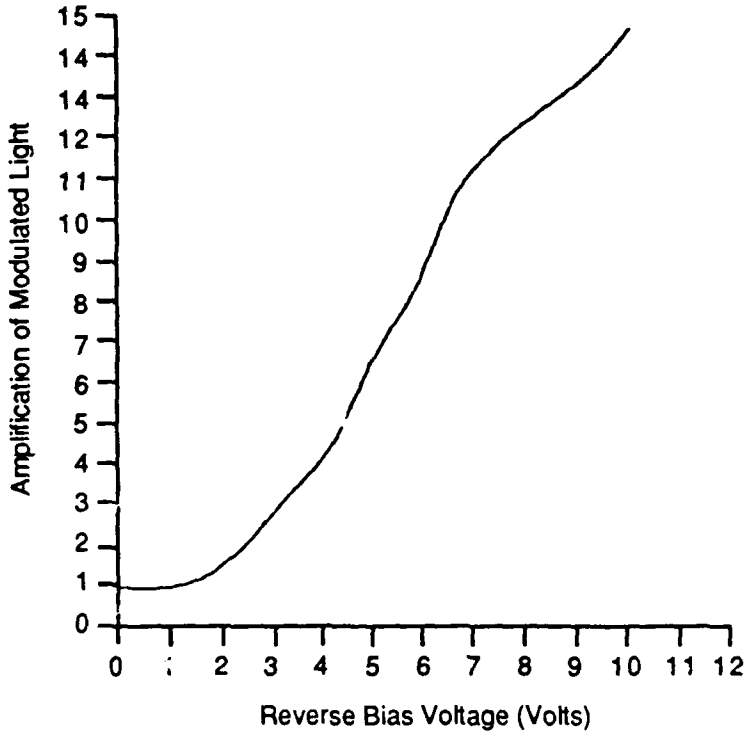

Figure 19
Amplification of Modulated Light as a Function of Reverse Bias Voltage with 632.8 nm Laser Shining on the Waveguide Surface; Dark Modulation at 12 Volt Reverse Bias. Voltage is Regarded as 1.

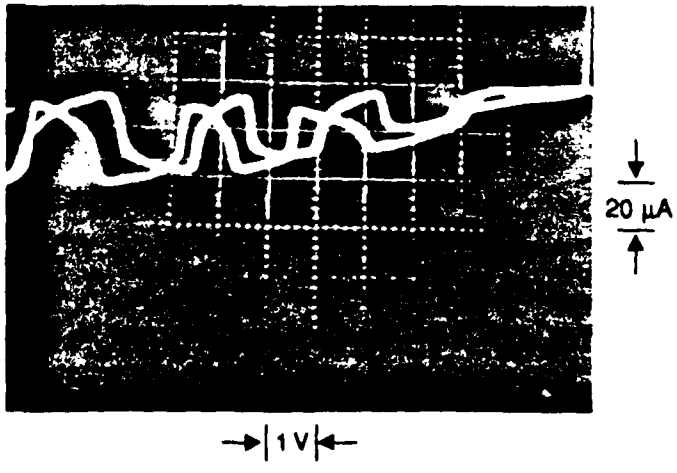

Figure 20
I-V Curve with 4 kHz Chopped Frequency

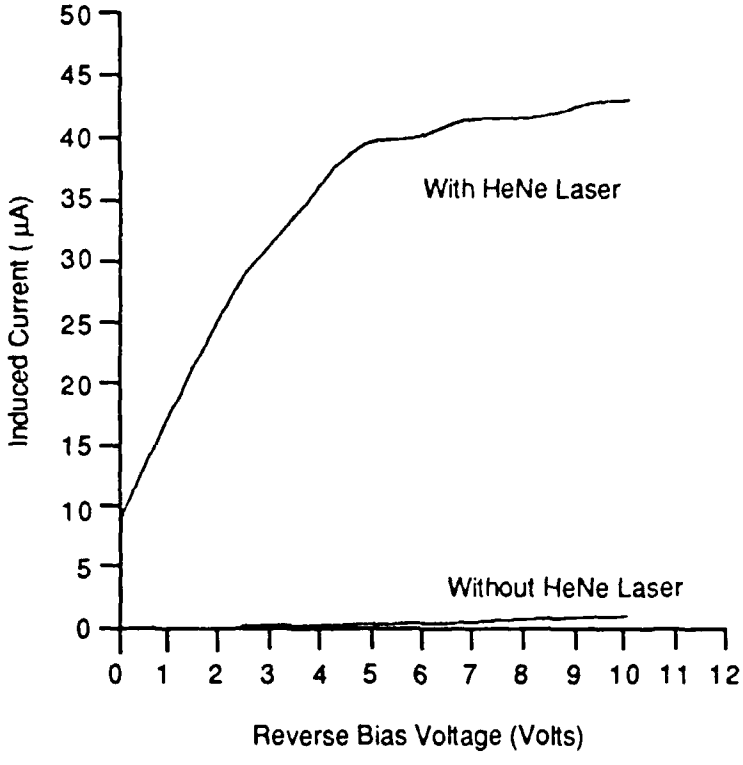

Figure 21
Induced Current as a Function of Reverse Bias Voltages With and Without a HeNe Laser (632.8 nm) Shining On the Window Area of the GaAs-GaAlAs Ridge Channel Waveguide

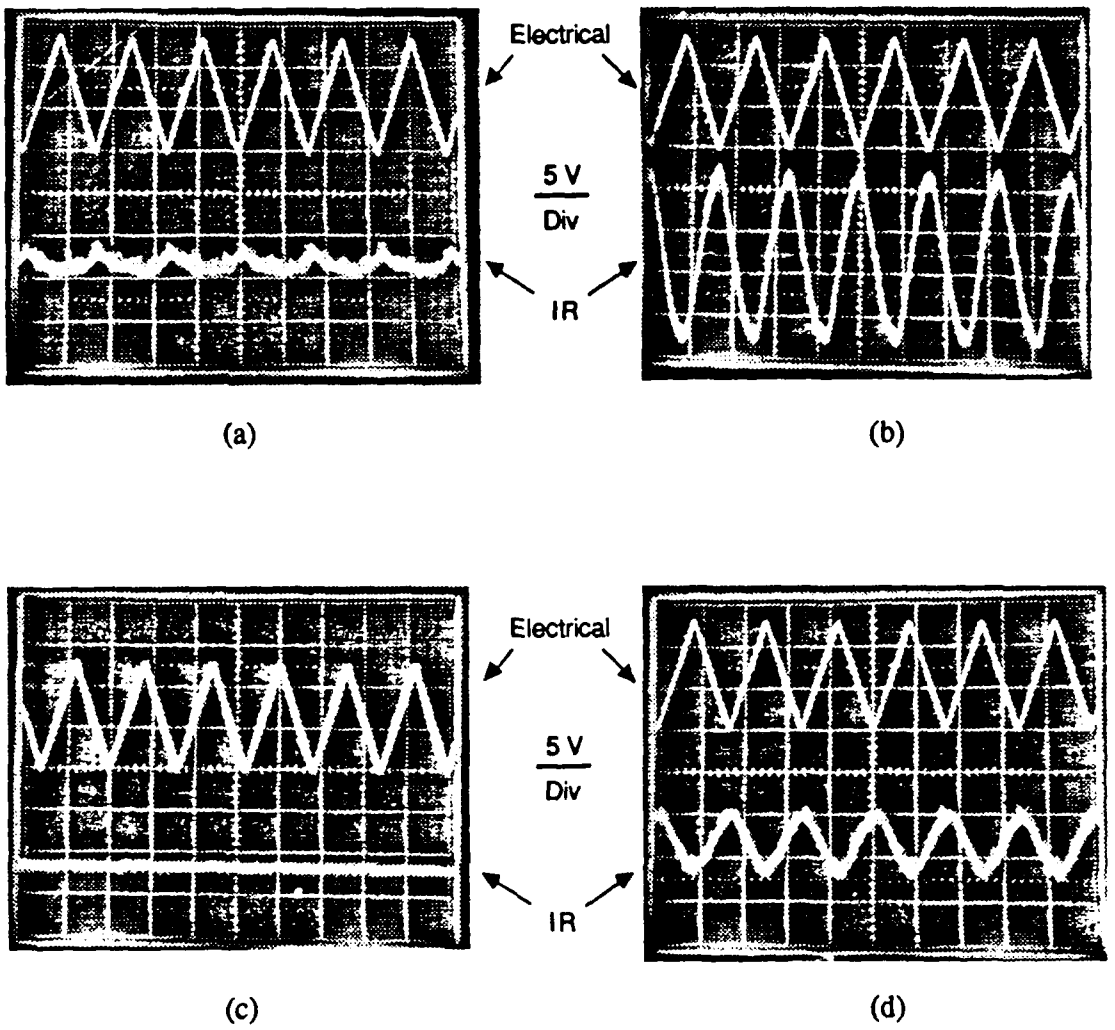

Figure 22
Modulated IR Guided Wave.
For TE Under (a) Purely Electrical Modulation Through the SMA Input Port (Figure 5), and (b) Optical Activated Modulation by Shining HeNe 632.8 nm Light on the Window. For TM Under (c) Purely Electrical Modulation Through the SMA Input Port (Figure 5) (for the Device Orientation Shown in Figure 1, No E-O Effect Exists for TM Mode), and (d) Optical Activated Modulation by Shining HeNe 632.8 nm Light on the Window. Modulation Enhancement is Clearly Shown in (b) and (d).

3.5 Modulation Speed

With respect to the modulation speed of the GaAs/GaAlAs channel waveguide OAM, the first limiting factor is the free carrier lifetime of the semiconductor material. For undoped GaAs, the carrier lifetime is around 10 ns [11]. Carrier lifetime in the picosecond and subpicosecond range has been achieved in GaAs by using doping or ion implantation techniques [12,13]. As a result of this achievement, the other limiting factor -- parasitic

RLC factors associated with electronic lumped structures -- shall be considered. Due to the limitation of the electronic equipment, the modulation speed was unable to be determined experimentally in Phase I. A theoretical calculation of the modulation bandwidth now follows. A detailed drawing of the complete device package is shown in Figure 23(a). The package includes a 50 ohm coaxial cable, a 50 ohm feed-through SMA connector, two bonding wires, a 50 ohm line, a device holder, two bonding pads and a waveguide modulator. The equivalent circuit corresponding to the complete device package is shown in Figure 23(b) with the related parameters indicated. A 50 ohm coaxial cable A is represented by R_S. The SMA connector with 50 ohm feed-through is represented by R_{ft}, B. L_1 and R_1 are, respectively, the inductance and resistance associated with the bonding wire C, R_d is the resistance corresponding to the 50 ohm stripe line D. L_2 is the inductance of the bonding wire H. R_2 is the combined resistance of the Au-plated chip carrier F, bonding wire H and the electrode bonding pad on GaAs G. The inductance of an Al wire is given by [25]

$$L = 2\phi\left[\ln\left(2\phi/r\right) - \delta\right] (nH) \tag{30}$$

where ϕ is the wire length, r is the wire radius and δ is the skin depth factor which is 0.75 when the length is much longer than the wire diameter. Based on Eq. (30), with $\phi = 0.5$ to 1 cm and $r = 100\ \mu m$, we have L_1 and L_2 in the range of 3.86 to 9.10 nH which is very close to the published data [26,27]. R_2 is determined to be within 0.035 to 0.07 ohm ($R = \rho \cdot \ell/A$, where ρ is the resistivity ($\rho = 2.8 \cdot 10^{-6}$ ohm/cm for Al), ℓ is the length and A is the area of the cross section). The resistance R_2 is dominated by the contact resistance of the Al electrode G and the bonding wire H. The combination of these is 0.21 to 0.25 ohm. The device capacitance C_s is a function of the carrier concentration and thus is directly related to the direct band gap of GaAs and $Ga_{1-x}Al_xAs$ compound semiconductor materials [28]. The direct band gap $E_g(x)$ of $Ga_{1-x}Al_xAs$ as a function of AlAs concentration can be represented as [28]

$$E_g(x) = \begin{cases} 1.424 + 1.247x & 0 < x < 0.45 \\ 1.424 + 1.247x + 1.147\,(x - 0.47)^2 & 0.45 < x < 1 \end{cases} \tag{31}$$

The variation of E_g as a function of x with x varying from 0.0 (GaAs) to 1.0 (AlAs) is shown in Figure 24. The heterostructure cutoff modulator was built with $GaAs/Ga_{0.93}Al_{0.07}As$ combination. The resultant variation of E_g is only 6%, which results in a difference of less than 3% in device capacitance. As a result, the device capacitance C_s can be accurately represented by the AlGaAs structure. For a Schottky barrier, the capacitance C_s is given by [29]:

$$C_s = \frac{\left(q \cdot \varepsilon_s \cdot N_d\right)^{0.5}}{\left(2\left(V_{bi} - V\right)\right)^{0.5}} \tag{32}$$

where q is the electric charge, ε_s is the dielectric constant, N_d is the donor concentration, and V_{bi} is the built-in voltage which is ~ 0.8 eV for metal/GaAs contact. The measured result at V = 0 volt gives a capacitance value of 1.1 pF and therefore, the voltage dependence of C_s can be written as

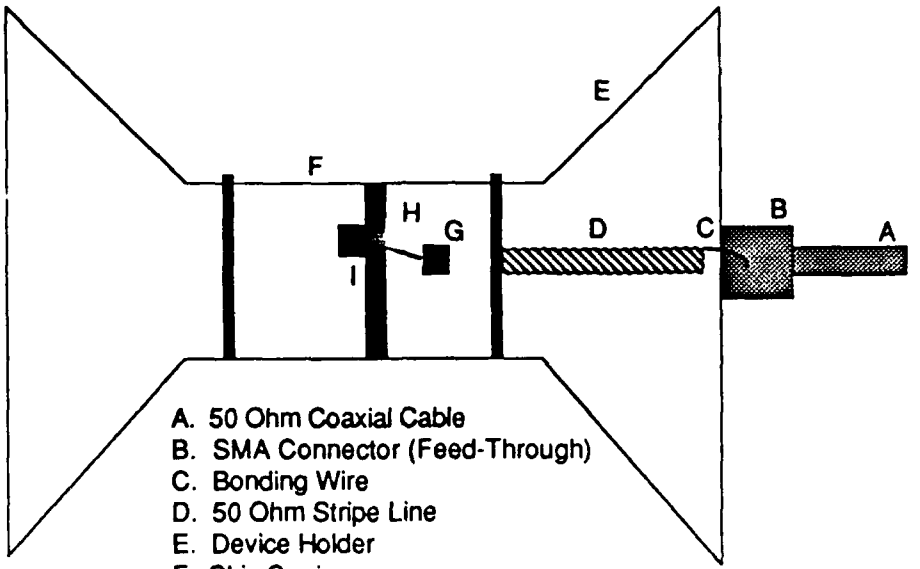

A. 50 Ohm Coaxial Cable
B. SMA Connector (Feed-Through)
C. Bonding Wire
D. 50 Ohm Stripe Line
E. Device Holder
F. Chip Carrier
G. Bonding Pad
H. Bonding Wire
I. Waveguide Modulator and Bonding Pad

(a)

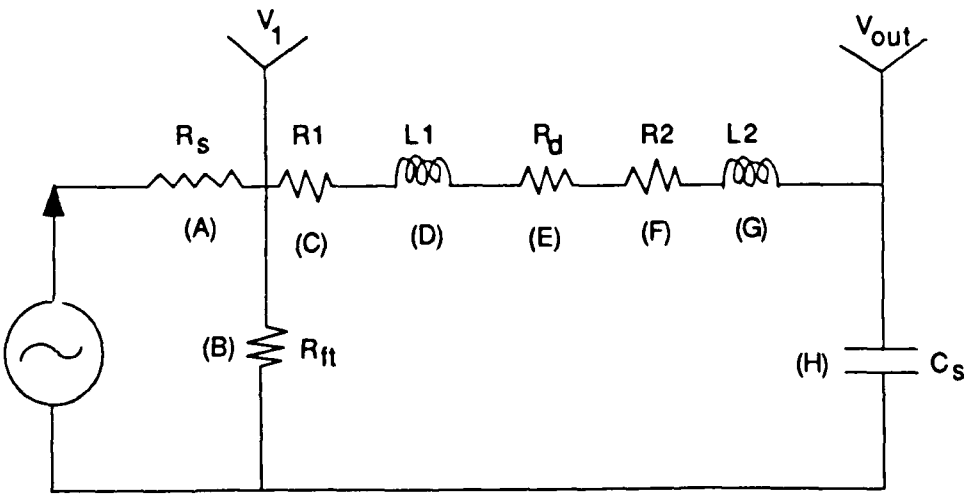

(b)

Figure 23
(a) Device Package of the GaAs-GaAlAs Single-Mode Optically-Activated Modulator and (b) Equivalent Circuit of the Device Package

$$C_s = \frac{(q \cdot E_s \cdot N_d)^{0.5}}{(2\,V_{bi})^{0.5}} \cdot \frac{1}{(1 - (V / V_{bi}))^{0.5}}$$

$$= 1.1 \cdot \frac{1}{(1 - (V / V_{bi}))^{0.5}} \quad \text{(pF)} \qquad (33)$$

in this specific case. The value of C_s as a function reverse bias voltage is depicted in Figure 25.

The modulation scheme for an electrooptic modulator involves the conversion of an input microwave signal to a modulated optical signal. To derive the output voltage response (transfer function), we first derive the voltage $V_1(\omega)$ (Figure 22) which can be represented as

$$V_1(\omega) = \frac{Z_{co}}{R_s + Z_{co}} \cdot V_{in} \qquad (34)$$

where

$$\frac{1}{Z_{co}(\omega)} = \frac{1}{R_{ft}} + \frac{1}{Z_t(\omega)} . \qquad (35)$$

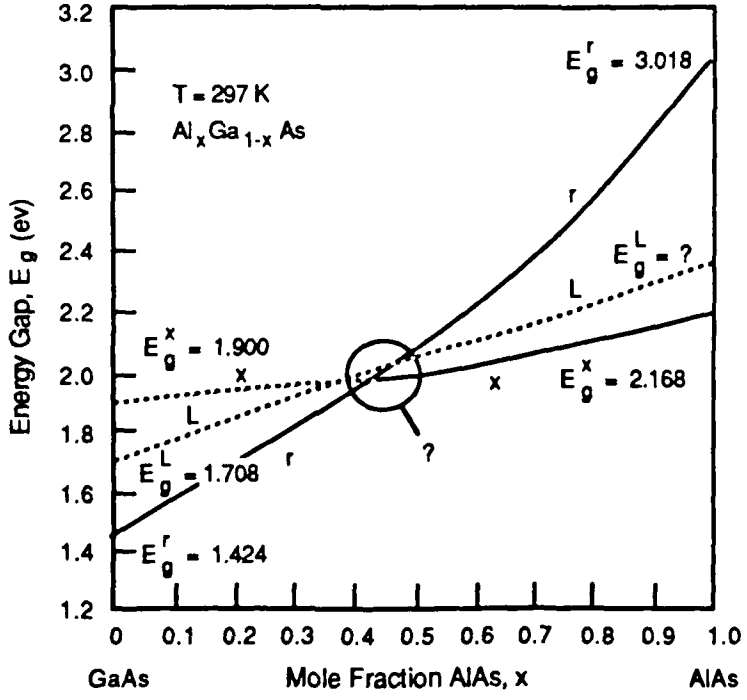

Figure 24
Compositional Dependence of the Direct Energy Gap and Indirect Energy Gap X and L for $Ga_{1-x}Al_xAs$

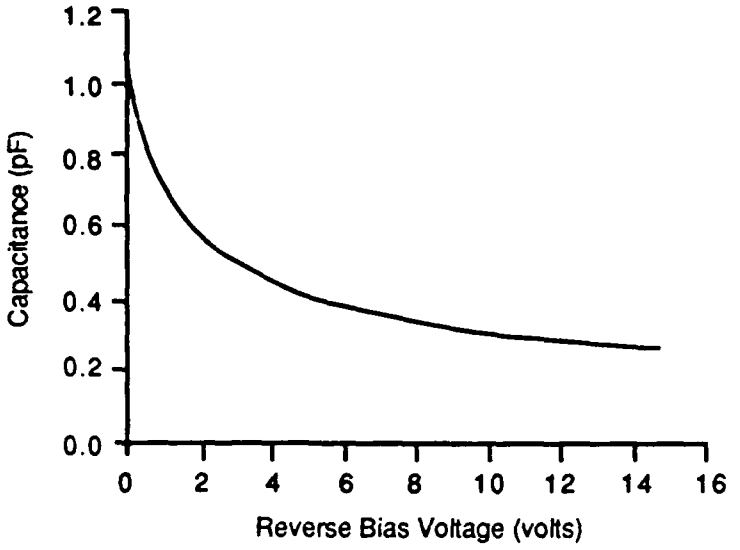

Figure 25
Device Capacitance as a Function of the Reverse Bias Voltage

In Eq. (35)

$$Z_t(\omega) = (R_1 + R_2 + R_d) + j(\omega L_1 + \omega L_2 - (1/\omega C_s)) \qquad (36)$$

ω in Eq. (36) is the angular frequency of the injected rf signal. The output voltage corresponding to Figure 22 is thus given by

$$V_{out}(\omega) = \frac{-j/\omega C_s}{(R_1 + R_2 + R_d) + j(\omega L_1 + \omega L_2 - (1/\omega C_s))} \qquad (37)$$

It is clear from Eq. (37) that the output voltage has a phase term which is a function of the rf frequency. By assigning the amplitude of V_{in} = 1 volt, the magnitude of V_{out} directly represents the output voltage response.

A computer simulation was made to evaluate the voltage and phase response as a function of the input rf frequency. The results are shown in Figures 26 and 27. Figure 26(a) and (b) represent the two extreme cases with the related parameters as shown. The correlation between voltage response V_1 with V_{out} (Figure 23) is also shown in these two figures. The phase response corresponding to Figures 26(a) and (b) is illustrated in Figures 27(a) and (b), respectively. The phase variation from Eq. (37) is clearly observed in these figures. The phase delay shown in these figures will be observed in explains the detected output phase shift shown on the oscilloscope.

As far as the lifetime of the optically generated free carriers is concerned, carrier lifetime in the picosecond to subpicosecond range was achieved in GaAs by using doping and ion implantation techniques [12,13]. Accordingly, the modulation speed is not limited by the current effect.

(a)

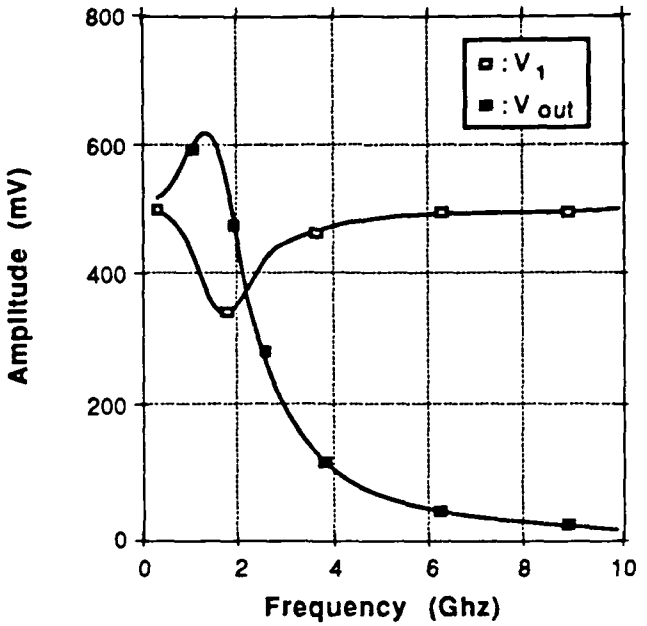

R_1 (Ohm)	L_1 (nH)	R_2 (Ohm)	L_2 (nH)	C_s (pF)
0.035	3.86	0.39	3.86	1.1

(b)

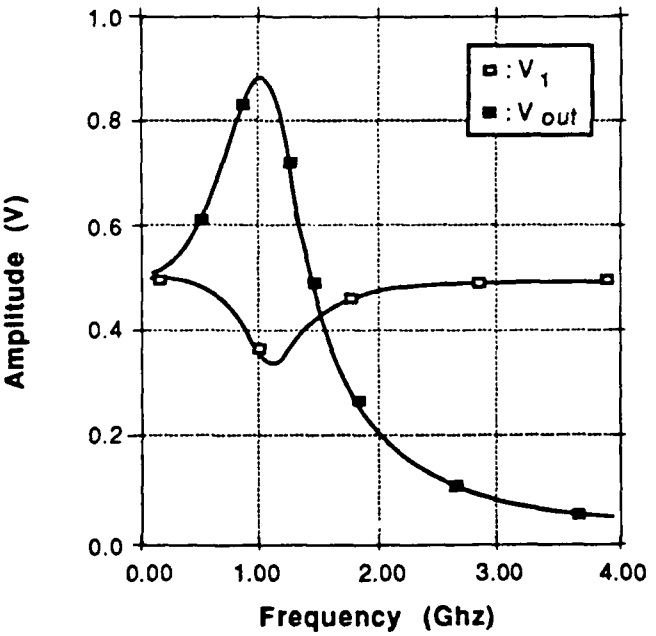

R_1 (Ohm)	L_1 (nH)	R_2 (Ohm)	L_2 (nH)	C_s (pF)
0.070	9.10	0.42	9.10	1.1

Figure 26
Computer Simulated Results of the Voltage Transfer Function of the Equivalent Circuit Shown in Figure 23 (V_1 and V_{out} are Defined in Figure 23(b)).

(a)

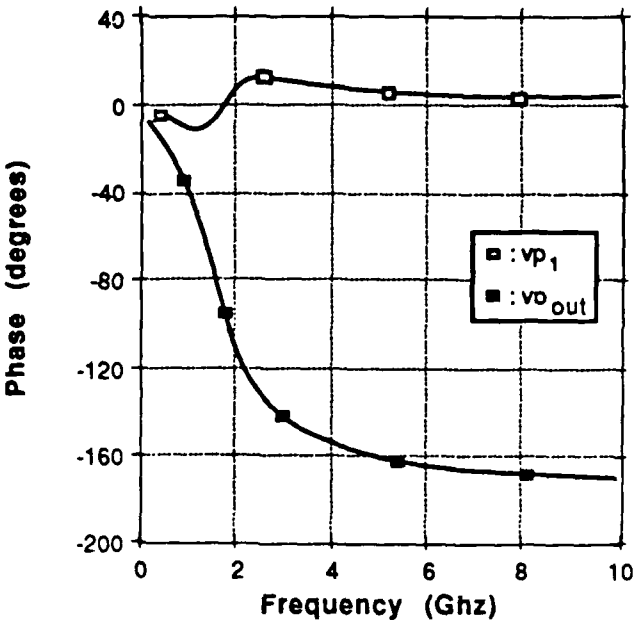

R_1 (Ohm)	L_1 (nH)	R_2 (Ohm)	L_2 (nH)	C_s (pF)
0.035	3.86	0.39	3.86	1.1

(b)

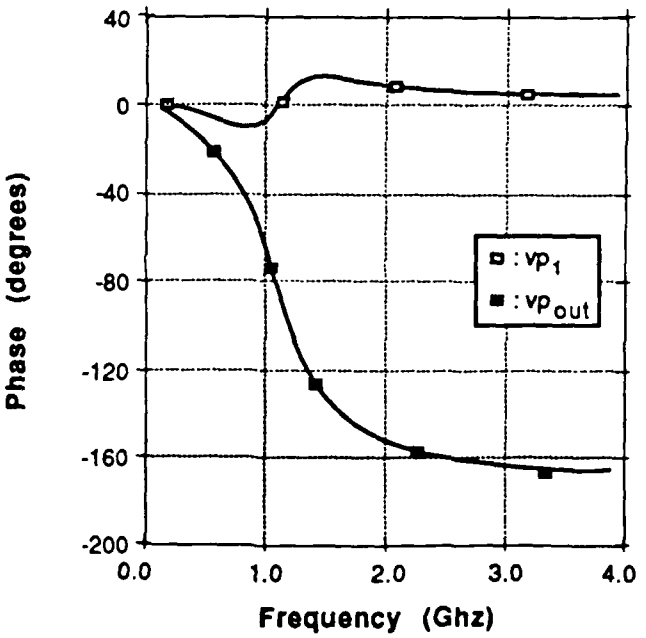

R_1 (Ohm)	L_1 (nH)	R_2 (Ohm)	L_2 (nH)	C_s (pF)
0.070	9.10	0.42	9.10	1.1

Figure 27
Computer Simulated Results of the Phase Response as a Function of the Input rf Frequency.

4.0 FURTHER APPLICATIONS

A variety of feasible applications for civilian and military electrooptic products are described in this section. The novel device structure proposed and then developed in this program has a number of SDIO-mission related applications. These include high-speed laser wavelength and incident direction sensors, IR countermeasure systems and crossbar switching devices. Other plausible devices and system applications are optical logic gates, ultra-short optical pulse generation, time division multiplexing and demultiplexing. All of these applications will be described in this section.

4.1 High-Speed Laser Wavelength and Incident Direction Sensors

Proliferation of laser weapons and laser guidance artillery has created a dangerous environment for both military personnel and equipment. Detecting of the wavelength and incident direction of laser radiation in a timely manner is a paramount issue in real time strategic defense. An optically activated modulator array working with a holographic band-pass filter plate, which POC has in-house capability to produce, is an excellent sensor system for application in this area. Figure 28 illustrates the concept of such a sensing system. For three-dimensional detection, the three parameters which need to be determined are wavelength, spherical angle θ, and azimuthal angle φ. The holographic band-pass filters associated with the GaAs OAM array have different center wavelengths. The two surfaces for the GaAs OAM array are located in the x-z and y-z planes. For each linear "pixel" p_j, the holographic band-pass filter has a center wavelength Λ_j. The linear arrays of the holographic filters project the incident light onto the two linear pixels of the GaAs OAM such that

$$\lambda \sin\theta \cos\varphi = \Lambda_a \tag{38}$$

$$\lambda \cos\theta = \Lambda_b \tag{39}$$

and

$$\theta = \tan^{-1}\left(\frac{d_2}{d_1}\right) \tag{40}$$

where Λ_a and Λ_b are the holographic rejection bands associated with planes 1 and 2, respectively, d_1 and d_2 are the distance projected (Figure 28). All these parameters can be experimentally determined through the OAM linear arrays. The unknown factors, i.e., λ, θ, and φ can be automatically determined through Eqs. (38) to (40). Note that the laser diode arrays and the detector arrays which are located at the input and output faces of the GaAs OAM arrays are not shown. The two linear pixels that are turned on by the incident laser beam can be detected by observing the intensity change of the OAMs through photodetectors.

Note that the results demonstrated in Phase I hold on <u>any semiconductor material</u>. Therefore, the range of wavelength detection can be adjusted by choosing an appropriate semiconductor material as the optically activated switching device. The size of each linear pixel is optimized such that low illumination intensity can be detected. For instance, a linear pixel of 5 cm (5 μm x 10^4) should be able to detect incident light in the μW region.

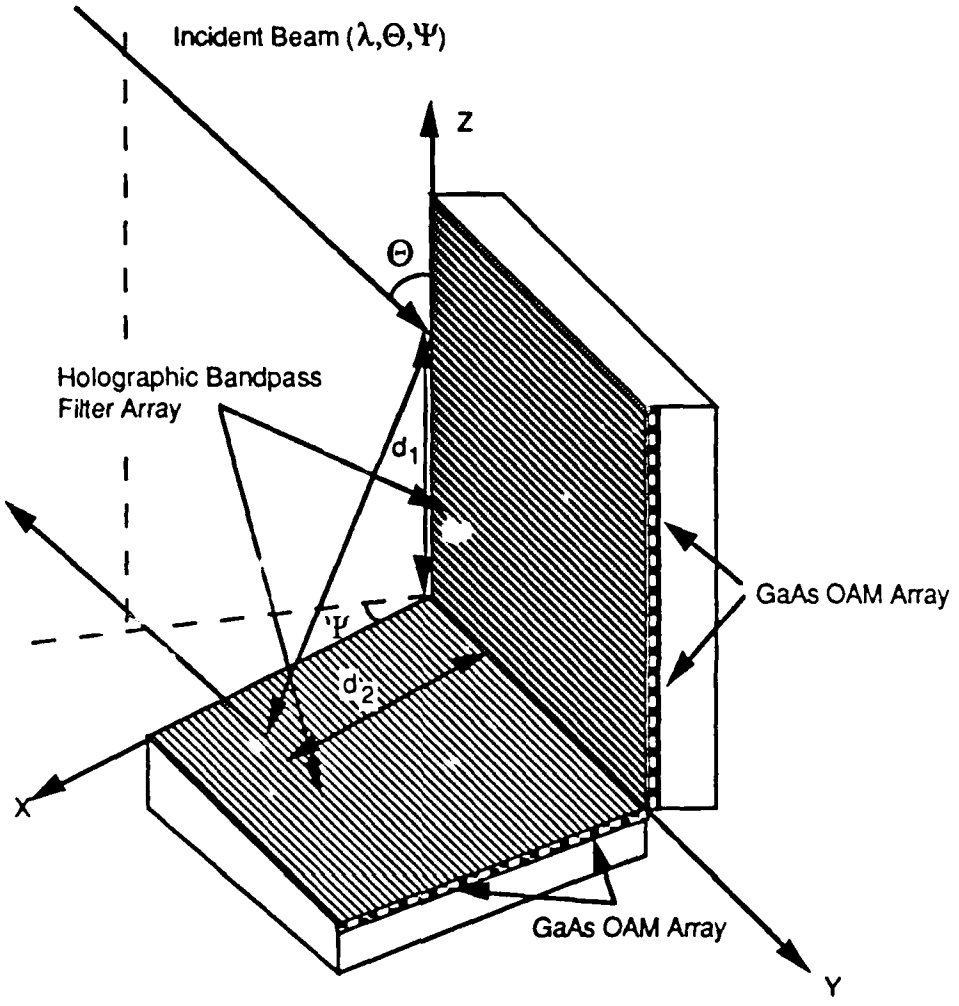

Figure 28
High Speed Laser Wavelength and Incident Direction Sensor

4.2 GaAs-OAM-Based IR Countermeasure System

To protect military vehicles from heat-seeking missiles, an IR modulator working within a spectral width of 3-to-5 μm can be made. Currently, such modulation is realized by (1) using an electrical chopper or (2) directly switching the power line on/off. These methods are not reliable because of the difficulty of changing the modulation speed and the slowness of the switching.

GaAs is transparent in these wavelengths. The proposed modulation concept will facilitate an excellent device for this application. Based on the described working principle, a GaAs-OAM-based IR countermeasure system is illustrated in Figure 29. The modulation speed is equivalent to that of the A-O Bragg cell. Modulation speed from kHz to GHz can be easily achieved by choosing an appropriate Bragg cell. The diffuser located at the output end is to enlarge the angle of view for the incoming missile.

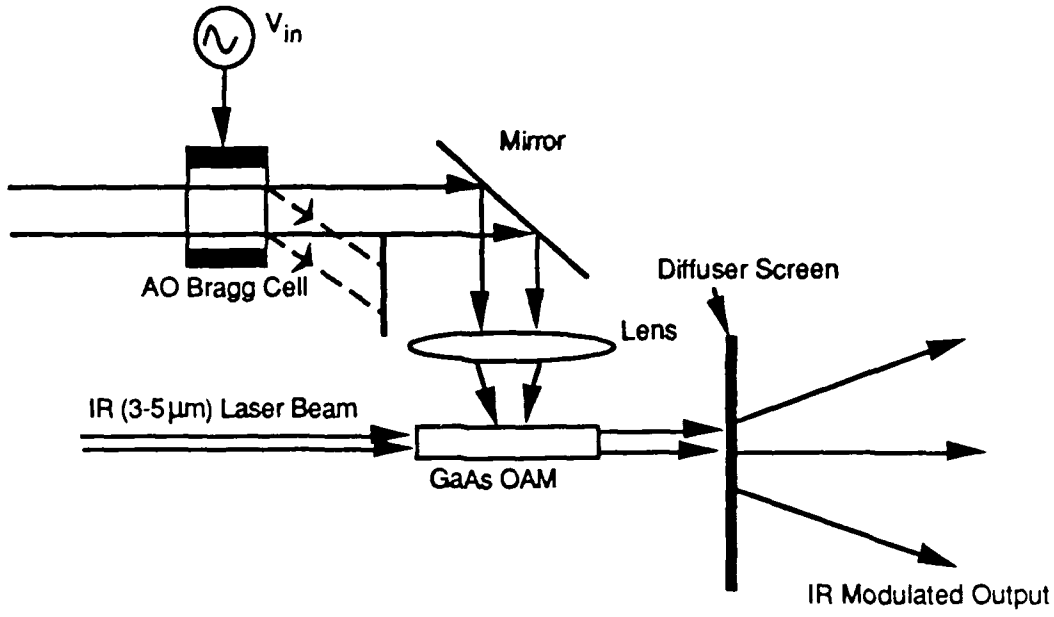

Figure 29
GaAs-OAM Based IR Countermeasure System

4.3 Low Threshold All-Optical Crossbar Switching Devices

Proliferation of electromagnetic pulse (EMP) and interference (EMI) effects requires an optical communication system without involving metallic electrodes to function as "antenna" in EMI- and EMP-copious environments. All-optical switching devices, based on $\chi^{(3)}$, i.e., the third order nonlinearity coefficient, need high power lasers in order to produce the required magnitude of index modulation. From a system point of view, such an approach is impractical. The GaAs-OAM arrays are an excellent candidate for this application. A schematic representation of the proposed concept is shown in Figure 30 where two linear arrays of GaAs-OAMs with 90° cross angles are shown. An n x n all-optical crossbar switch is portrayed. The detailed cross section explains the working principle of the device. Similar to the circular window shown in Figure 7, the optical window has a "grating-type" transmission mask. The all-optical grating can be activated by visible light illumination. When the optical activation source (similar to Figure 1, not shown here) is off, the IR optical guided wave incident from port 1 will exit the device out of port 3 (Figure 30) and likewise light entering port 2 will exit out of port 4. When an optical activation source is turned on, the all-optical grating is generated through free-carrier induced index modulation. The all-optical grating will automatically shift the guided wave input from port 1 to output port 4 and input port 2 to output port 3 due to the pre-designed phase-matching condition

$$\Lambda = \frac{\lambda}{2\, N_{eff} \cos 45°} \tag{41}$$

where Λ is the mask spacing for all the optical grating, and λ and N_{eff} are the IR signal carrier wavelength and the guided mode effective index, respectively. Note that the activation source can be a two-dimensional LED array which is compact in size and low in cost. The length of the all optical grating region d can be easily optimized by

implementing a horn structure such that the product of Δn (optical induced index change) and d is properly manipulated.

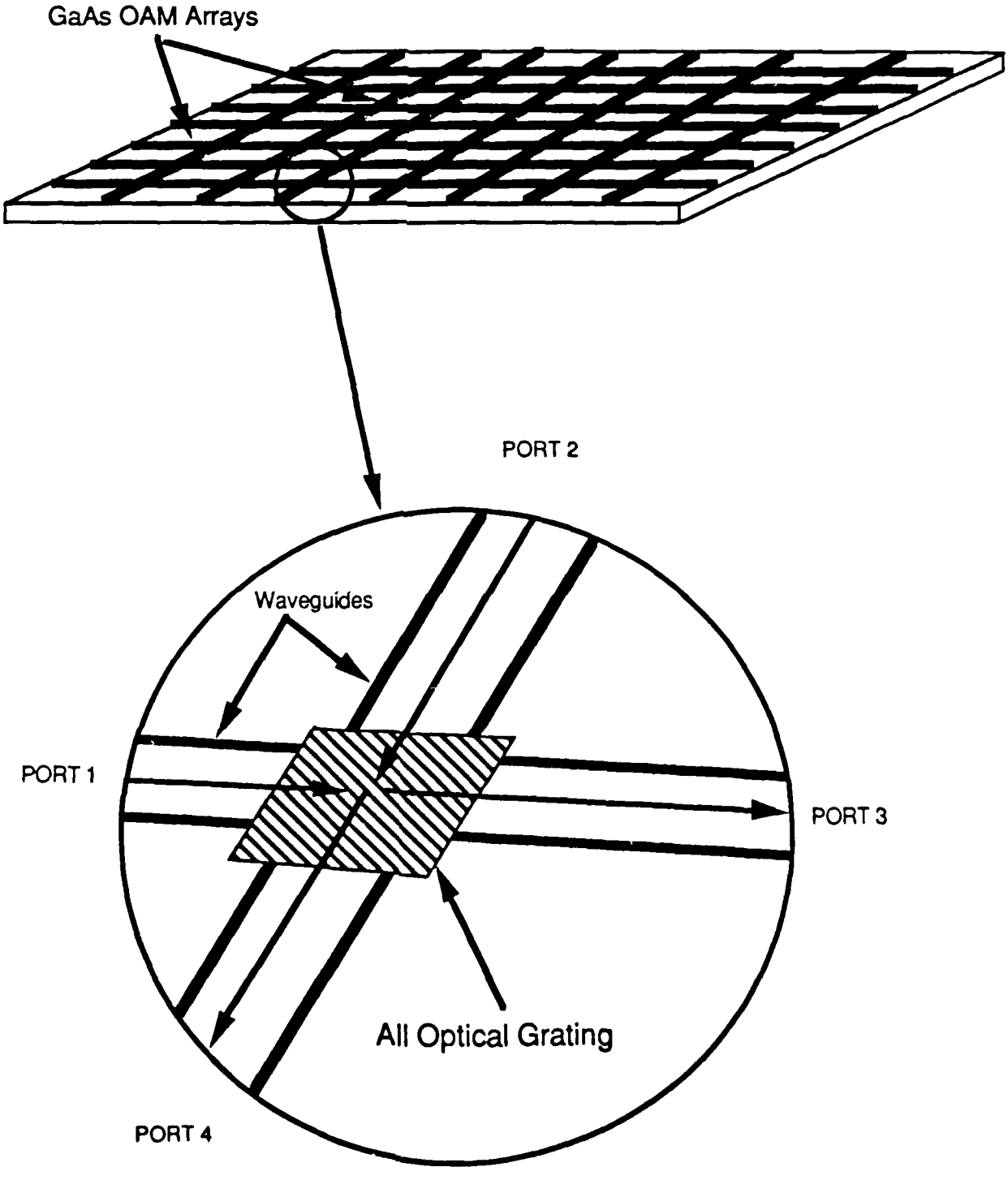

Figure 30
Low Threshold All Optical Crossbar Switching Device

4.4 Optical Gates

GaAs OAMs working in both the phase- and cutoff-regimes can be used as optical gates. An all-optical OR gate using the 0.63 μm optical wave and an electrical signal added through the SMA connectors as the two logic input and the optical throughput (1.3 μm IR guided wave) as the logic output is shown in Figure 31. The truth table is also included. The only condition that the output logic level shifts to 0 is when A, i.e., 0.63 μm light and B, i.e., electrical signal are both at the 0 state. Note that the throughput intensity for A and B both equal to 1 is higher than A = 0/B = 1 and A =1/B = 0. This discrepancy can be eliminated by setting the threshold level of the photodetector. Realization of an optical NOT gate is easily realized using 0.633 μm light as the input gate signal and a 1.3 μm guided wave as the output gate signal.

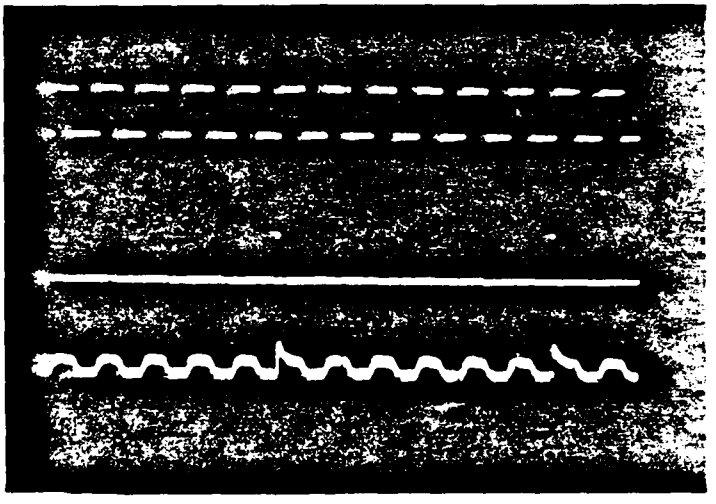

Truth Table

A	0	1	0	1
B	0	0	1	1
C	0	1	1	1

Figure 31
Optical OR Gate Using GaAs OAM Working in the Phase Modulation Regime

By biasing an optically activated GaAs cutoff modulator at a suitable reverse voltage and applying the logic inputs at the multiple sections of the Schottky electrode (as depicted in Figure 32), NOT, OR, and AND gates [30] are successfully realized. The gate inputs are electrical signals and the gate output is the throughput light of the guided wave. The NOT gate is easily realized by using the input voltage to cut off the throughput light. Whenever the input signal is on ($V \geq V_c$ (cutoff voltage)), the throughput is at minimum intensity, i.e., cutoff, which is defined as 0; otherwise it is 1. The optical OR gate is fulfilled by

biasing the device in the cutoff region. Without any input, i.e., A = B = 0 where A and B designate the input signals, the throughput is at a minimum, and therefore, we have Y(output) = 0. However, whenever A = 1 and/or B = 1, the operating point of the modulator of the transfer curve is shifted to a region with significant throughput light. We thus have Y = 1. The result of the OR gate is shown in Figure 33. Figures 33 (a), (b), and (c) display, respectively, the results with A = 1, B = 0, A = 0, B = 1, and A = B = 1. The discrepancy in the throughput intensity of the Y = 1 state for A = B = 1 and A = 1, B = 0 (or A = 0, B = 1) is due to the different operating points involved. This discrepancy may be removed by setting the proper saturation level of the detector. In the case of the optical AND gate, the device is biased to a region that is well below the cutoff so that only when A = B = 1 will the throughput light become significant.

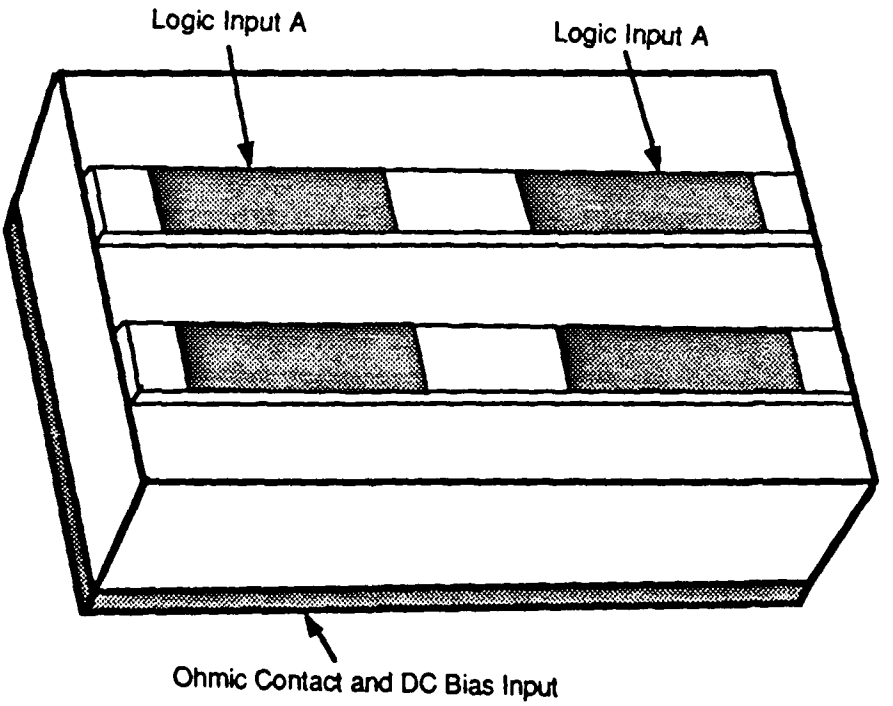

Figure 32
Electrode Arrangement for Logic Gate Applications

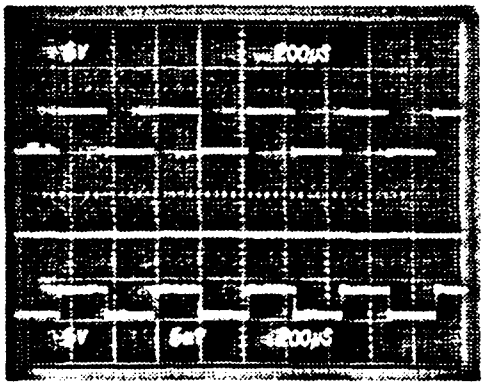

A = 1

B = 0

Y = 1

(a)

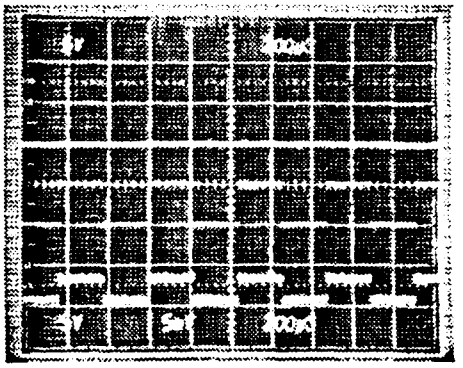

A = 0

B = 1

Y = 1

(b)

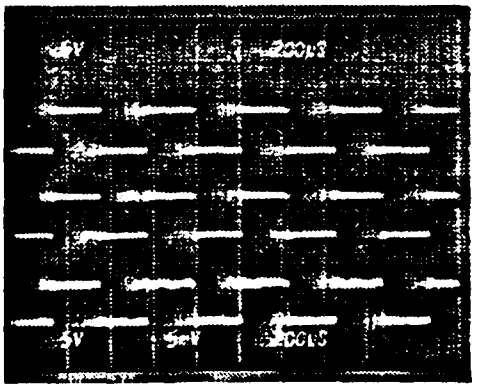

A = 1

B = 1

Y = 1

(c)

Figure 33
The Measured Results of Optical OR Gate: (a) A = 1, B = 2, Y = 1; (b) A = 0, B = 1, Y = 0; and (c) A = B = 1, Y = 1. The Result of A = B = 0, Y = 0 is Shown in All Pictures.

4.5 Data Sampling and Encoding, Generation of Very Short Optical Pulses, and Time Division Multiplexing

Optical data sampling was easily realized by applying a DC bias and an rf modulation signal to the GaAs channel waveguide modulator. The laser light coupled into the waveguide was externally modulated first. The data to be sampled is controlled by the proper input sampling signal. The result depends upon the waveform of the sampling signals. Also, when proper gating signals are applied to the multiple modulation electrodes, the modulator can be used to generate a jitter-free train of very short light pulses for application in a high-speed sampling oscilloscope [31], to measure the speed of a fast electrooptic switch/modulator by means of a low speed detector [32], and to construct an electrooptic sampling system for high frequency optical waveform display [33]. The approach for generating such short optical pulses will now be explained. Four different microwave signals are individually added to the electrode pads shown in Figure 34. The frequencies of the input microwave signals are ω, 2ω, 3ω, and 4ω, respectively. If we bias the device in the linear region of the transfer curve of the device, the modulated optical signal due to the combination of these four microwave signals is

$$I_{op} = I_t \cdot \sin(\omega t + \varphi_1) \cdot \sin(2\omega t + \varphi_2) \cdot \sin(3\omega t + \varphi_3) \cdot \sin(4\omega t + \varphi_4) \qquad (42)$$

where I_t is the throughput intensity without an external AC field and sin $(\omega t + \varphi_1)$, sin $(2\omega t + \varphi_2)$, sin $(3\omega t + \varphi_3)$, and sin $(4\omega t + \varphi_4)$ are microwave signals applied to four different electrode pads of the same optical channel. φ_1, φ_2, φ_3, and φ_4 are the delay times that include the transmit time delay of the guided wave and the microwave propagation delay. The desired delay times can be adjusted through selection of the proper length coaxial cables or using line stretchers. The proper delay time is chosen such that

$$\varphi_1 = \varphi_2 = \varphi_3 = \varphi_4 = \pi/2 \qquad (43)$$

Under this condition, the modulated optical output intensity can be easily derived through simple calculation. The result is shown in Eq. (44) which gives

$$I_{op} = I_t \cdot 64\,[\cos(\omega t)]^{10}. \qquad (44)$$

The output in this condition is the tenth power of cos (ωt). To clarify the condition, a computer simulated optical output and the fundamental mode of microwave input signal are both shown in Figure 35. A very sharp pulse can be generated using this method. If the fundamental frequency of the microwave signal is ω = 1 GHz, an optical pulse with ~100 picosecond 3 dB pulse width can be generated. An even shorter optical pulse can be generated with a higher fundamental microwave frequency. The relationship of the fundamental microwave frequency and the 3 dB optical pulse width is depicted in Figure 36. The desired output optical pulse width can be acquired by injecting suitable combinations of microwave signals.

Encoding and time-division multiplexing of multi-channel signals on an optical wave can also be accomplished by applying the signals to the multiple sections of the modulating electrode formed on a single ridge channel waveguide (see Figures 34 and 5). Time-division multiplexing of four channels using a modulator with four electrode sections, each 1 mm long, has been carried out. Figure 37 shows the multiplexed waveform of two, three and four channels each with a 10 ns pulse train. The time delays of each pulse

sequence are adjusted externally. Clearly, the number of channels to be multiplexed can be greatly increased by utilizing the modulator array together with a waveguide lens fabricated in the same GaAs substrate. Note that GaAs OAMs working in the phase- and cutoff-regimes are both useful for TDM application. However, it should be emphasized that the GaAs optically activated cutoff modulators presented in this section can utilize both coherent and incoherent light sources in all of the applications referred to above. Demultiplexing of the TDM signals can be realized by utilizing the OAM device shown in Figure 38 at the receiving port.

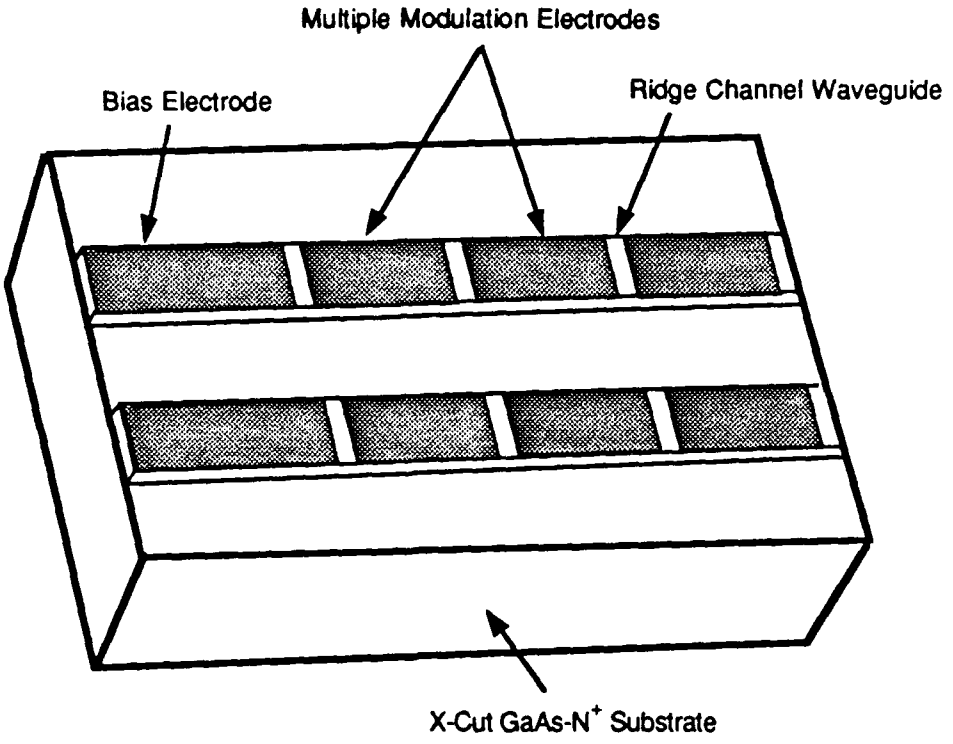

Figure 34
Electrode Arrangement for Multiple-Channel Applications of the GaAs-GaAlAs Heterostructure Cutoff Modulator Array

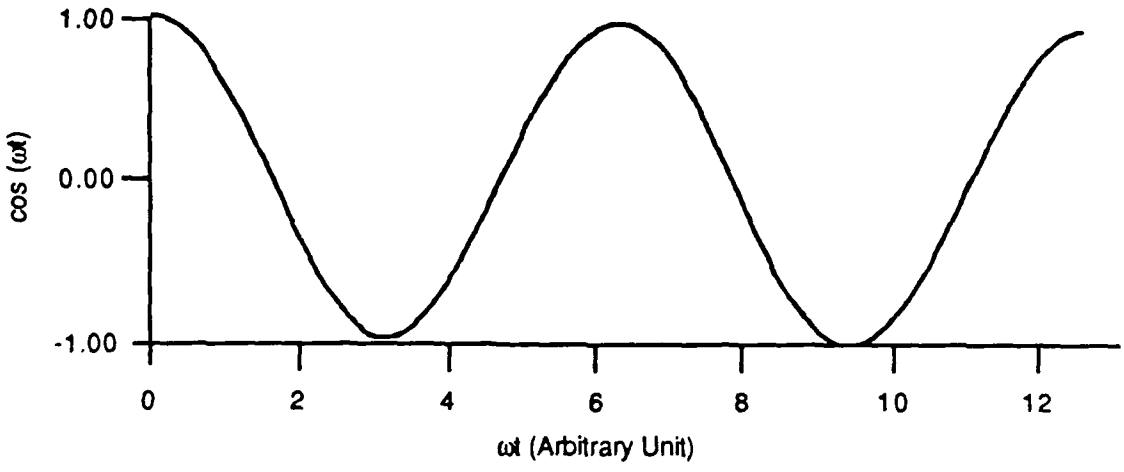

(a)

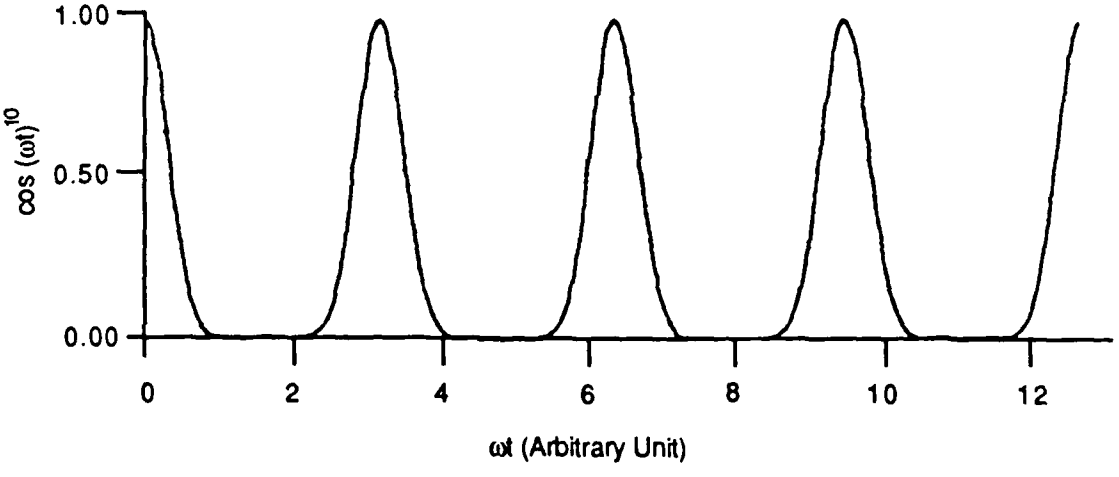

(b)

Figure 35
The Calculated Results of the Jitter-Free Optical Pulse: (a) Fundamental Mode cos (ωt) and (b) the Generated Optical Pulses [cos $(\omega t)^{10}$]

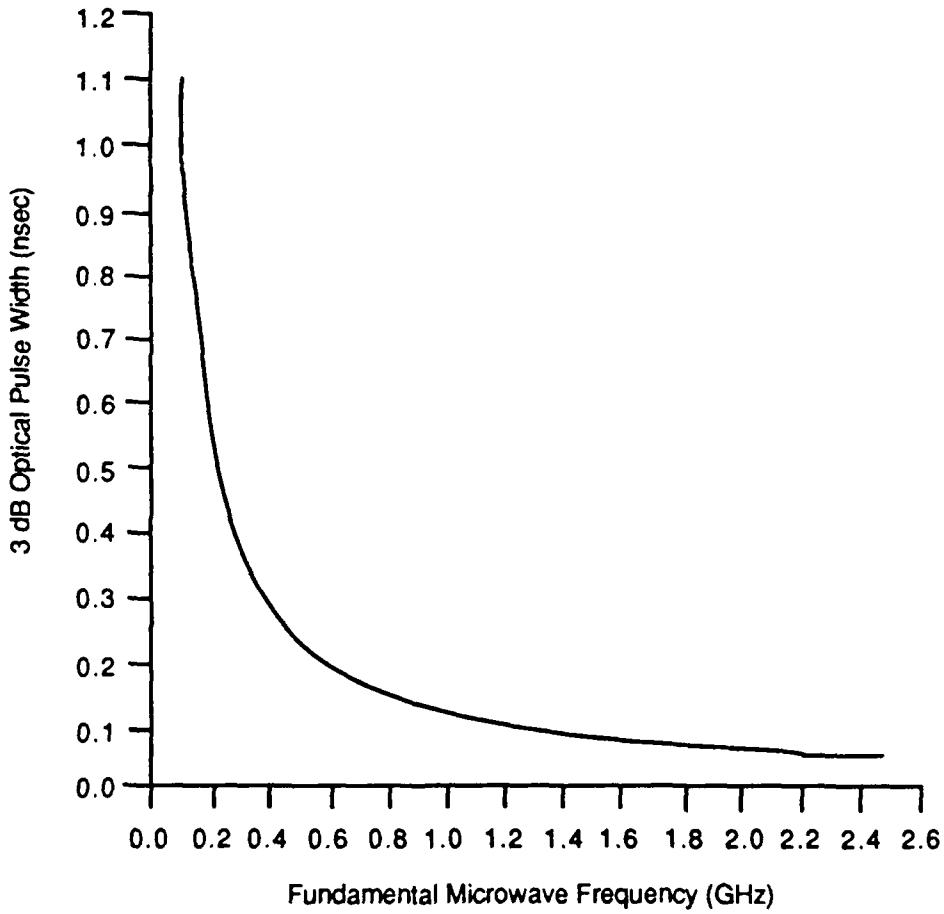

Figure 36
Calculated Pulse Width as a Function of Fundamental Mode Microwave Frequency

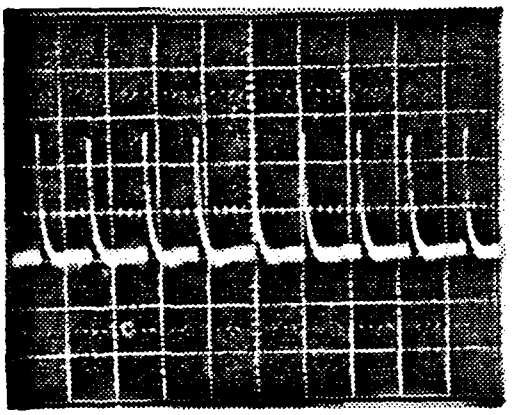

(a)

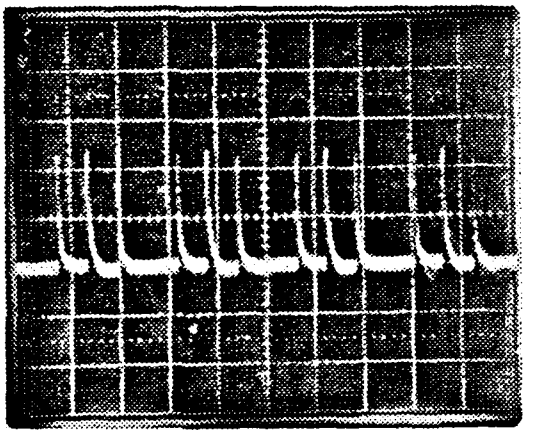

(b)

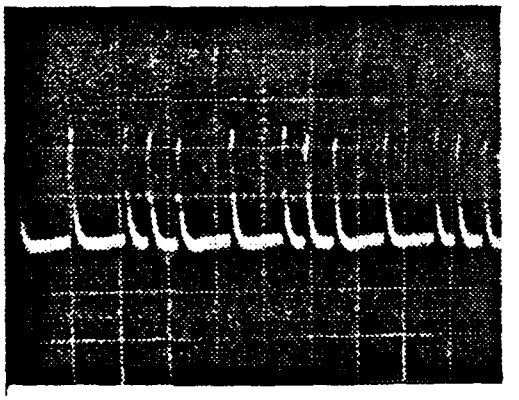

(c)

Figure 37
The Multiplexing of Multi-Electrical Pulse Trains: (a) Two Pulse Trains, (b) Three Pulse Trains, and (c) Four Pulse Trains. The Pulse Width is 10 nsec.

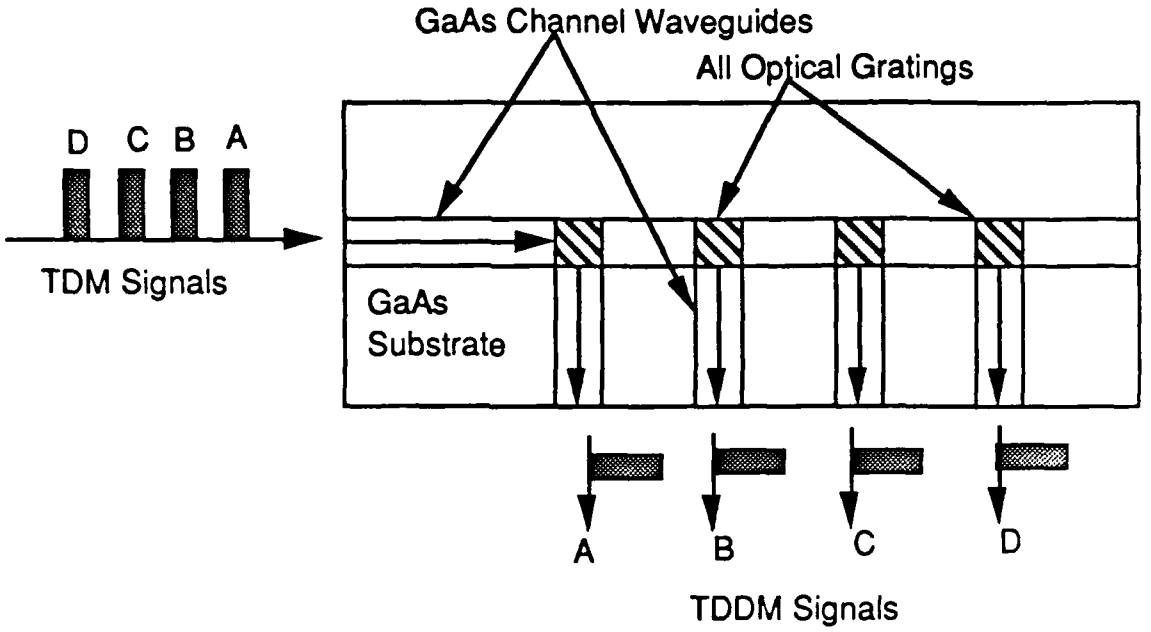

Figure 38
Demultiplexing of the TDM Signals Using the Proposed OAM

5.0 CONCLUSIONS

We present for the first time, to the best of our knowledge, an optically activated modulator (OAM) on a GaAs/GaAlAs heterostructure channel waveguide. Experimental results show that a device interaction length shorter than that of MQWs is capable of producing an OAM device with 8.2 dB modulation depth. Theoretical calculations are provided to compare the index modulation between optical activation and the linear electrooptic effect. Experimental work was also conducted to confirm the magnitude of the optically-generated index modulation through free-carrier injection. The single-mode GaAs OAM device can be designed either as a phase modulator or as a cutoff modulator. A theoretical calculation based on the variation of the confinement factor as a function of the guided mode effective index is provided. Design criterion for both cases is given. Optically activated modulators using GaAs/GaAlAs channel waveguides were fabricated. Fully packaged devices were demonstrated for both single-channel OAMs and OAM arrays. Optically activated modulation was demonstrated in both phase modulation and cutoff modulation regimes. Signal multiplexing was further conducted using optical activation sources, IR signal carriers and electrical signals. The modulation speed/bandwidth was also considered and the results showed a multi-Gigahertz device operational bandwidth. Improvement of modulation speed is feasible by employing a traveling wave electrode structure on a semi-insulating substrate. Finally, further applications based on GaAs OAMs and OAM arrays, including laser wavelength and incident direction sensors, IR countermeasure systems, all optical EMI- and EMP-free crossbar switches, optical logic gates (NOT, OR and AND gates), short optical pulse generation, and time division multiplexing are further introduced. The OAM we proposed and then developed in Phase I is an attractive device for both SDI-related and civilian applications. As a result, Phase III product development is expected to yield useful devices for the optoelectronic industry.

6.0 REFERENCES

1. M. Papuchon, et al., "Electrically Switched Optical Directional Coupler: Cobra," Appl. Phys. Lett., 27, 289 (1975).

2. R. C. Alferness, R. V. Schmidt, and E. H. Tuner, "Characterization of Ti-Diffused $LiNbO_3$ Optical Directional Couplers, Appl. Opt., 18, 4012 (1979).

3. W. E. Marin, "A New Waveguide Switch/Modulator for Integrated Optics," Appl. Phys. Lett., 32, 562 (1975).

4. V. Ramaswamy, M. D. Divino, and R. D. Standley, "Balanced Bridge Modulator Switching Using Ti-Diffused $LiNbO_3$ Strip Waveguides," Appl. Phys. Lett., 32, 644-646 (1978).

5. C. L. Chang and C. S. Tsai, "Electrooptic Analog-to-Digital Convertor Using Channel Waveguide Fabry-Perot Modulator Array," Appl. Phys. Lett., 43, 22 (1983).

6. S. Y. Wang, S. H. Lin, and M. Huong, "GaAs Traveling-Wave Polarization Electro-Optic Waveguide Modulator with Bandwidth in Excess of 20 GHz at 1.3 μm," Appl. Phys. Lett., 51, 83 (1987).

7. R. T. Chen, "E-O Depolarization Switch on Y-Cut $LiNbO_3$ PE Channel Waveguides," Appl. Phys. Lett., 54, 2628 (1989).

8. R. Chen and C. S. Tsai, "Thermally Annealed Single-Mode Proton-Exchanged Channel Waveguide Cut Off Modulator," Opt. Lett., 11, 546 (1986).

9. R. Chen, "Thermally Annealed Mode Annihilation Switching Array on Proton Exchanged $LiNbO_3$ Channel Waveguides," SPIE, San Diego, CA, 1989.

10. R. Chen, et al., "GaAs-GaAlAs Heterostructure Single-Mode Channel Waveguide Cutoff Modulator and Modulator Array," IEEE J. of Quantum Electron., QE-23, 2205 (1987).

11. S. M. Sze, Physics of Semiconductor Devices, 2nd ed., p. 851 (John Wiley & Sons, 1981).

12. See, for example, D. H. Auston, Appl. Phys. Lett., 26, 101 (1975); J. A. Buck, K. K. Li, and J. R. Whinnery, J. of Applied Physics, 51, 769 (1980); P. Cheung, et al., IEEE Trans Microwave Theory and Tech., 38, 586 (1990); and C. H. Lee, IEEE Trans Microwave Theory and Tech., 38, 596 (1990).

13. M. B. Johnson and T. C. McGill, Appl. Phys. Lett., 54, 2424 (1989).

14. R. A. Soref and B. R. Bennett, "Electro-Optic Effects in Silicon," IEEE J. of Quantum Electron., QE-23, 123 (1987).

15. J. P. Lorenzo and R. A. Soref, "1.3 mm Electro-Optic Silicon Switch," Appl. Phys. Lett., 51, 6 (1987).

16. J. Manning, R. Olshansky, and C. B. Su, "Strong Influence of Nonlinear Gain on Spectral and Dynamic Characteristics of InGaAsP Laser", Electron. Lett., 21, 496 (1985).

17. N. K. Dutta, N. A. Olsson, and W. T. Tsang, "Carrier Induced Refractive Index Change in AlGaAs Quantum Well Lasers," Appl. Phys. Lett., 45, 836 (1984).

18. K. Tada and Y. Okada, "Bipolar Transistor Carrier-Injected Optical Modulator/Switch: Proposal and Analysis," IEEE Electron. Device Lett., EDL-7, 605 (1986).

19. O. Mikami and H. Nakagome, "Waveguide Optical Switch in InGaAs/InP Using Free-Carrier Plasma Dispersion," Electron. Lett., 20, 228 (1984).

20. K. Ishida, H. Nakamura, R. Matsumura, T. Kadoi, and H. Inoue, "InGaAsP/InP Optical Switches Using Carrier Induced Refractive Index Change," Appl. Phys. Lett., 50, 141 (1987).

21. N. W. Ashcroft, et al, Solid State Physics (Cornell University, Ithaca, NY, 1976).

22. Personal communication with Dr. R.A. Soref from RADC, September 1989.

23. B. G. Streetman, Solid State Electronic Devices, (Prentice-Hall, Inc., Englewood Cliffs, NJ, 1980).

24. Purchased from Epitronics, Arizona.

25. "Lead Inductance Comparisons," Semiconductor International, 74 (June 1988).

26. J. L. Nightingale, R. A. Becker, P. C. Willis, and J. S. Vrhel, "Characterization of Frequency Dispersion in Ti-Indiffused $LiNbO_3$ Optical Devices," Appl. Phys. Lett., 51, 716 (1987).

27. Xin Cheng, "Thin Film Characterization and Electrooptic Bragg Modulator," Ph.D. Dissertation, University of California, 1987.

28. H. C. Casey, Jr., and M. B. Panish, Heterostructure Laser, Vol. 1, (John Wiley and Sons, 1984).

29. S. M. Sze, Physics of Semiconductor Devices, Chapter 4, Part III, (John Wiley and Sons, 1983).

30. H. F. Taylor, "Guided Wave Electrooptic Devices for Logic and Computation," Appl. Opt., 17, 1493 (1978).

31. H. A. Haus, S. T. Kirsch, K. Mathyssek, and F. J. Leonberger, "Picosecond Optical Sampling," IEEE J. of Quantum Electron., QE-16, 870 (1980).

32. R. C. Alferness, N. P. Economou, and L. L. Buhl, "Picosecond Optical Sampling Technique for Measuring the Speed of Fast Electrooptic Switch/Modulators," Appl. Phys. Lett., 37, 597 (1980).

33. Janis A. Valdmanis, and G. Mourou, "Subpicosecond Electrooptic Sampling: Principles and Applications," IEEE J. of Quantum Electron., QE-22, 69 (1986).